Late Holocene glacial advance and ice shelf growth in Barilari Bay, Graham Land, west Antarctic Peninsula

Andrew J. Christ[1,†], Manique Talaia-Murray[1], Natalie Elking[1], Eugene W. Domack[1,§], Amy Leventer[2], Caroline Lavoie[3,#], Stefanie Brachfeld[4], Kyu-Cheul Yoo[5], Robert Gilbert[6], Sun-Mi Jeong[5], Stephen Petrushak[7], Julia Wellner[8], and the LARISSA Group[9]

[1]*Department of Geosciences, Hamilton College, Clinton, New York 13323, USA*
[2]*Department of Geology, Colgate University, Hamilton, New York 13346, USA*
[3]*Istituto Nazionale di Oceanografia e di Geofisica Sperimentale (OGS), Borgo Grotta Gigante, Sgonico 34010, Italy*
[4]*Department of Earth and Environmental Studies, Montclair State University, Montclair, New Jersey 07043, USA*
[5]*Korean Polar Research Institute, Incheon, 406-840, Republic of Korea*
[6]*Department of Geography, Queen's University, Kingston, Ontario K7L 3N6, Canada*
[7]*Antarctic Research Facility, Florida State University, Tallahassee, Florida 32306-4100, USA*
[8]*Department of Earth and Atmospheric Sciences, University of Houston, Houston, Texas 77204, USA*
[9]*The LARISSA (Larsen Ice Shelf System, Antarctica) Group includes G. Balco, S. Brachfeld, M. de Batist, E. Domack, A. Gordon, T. Haran, J.-P. Henriet, B. Huber, S. Ishman, S. Jeong, M. King, C. Lavoie, A. Leventer, M. McCormick, E. Mosley-Thompson, E. Pettit, T. Scambos, C. Smith, L. Thompson, M. Truffer, C. van Dover, M. Vernet, J. Wellner, K. Yu, and V. Zagorodnov*

ABSTRACT

Three marine sediment cores were collected along the length of the fjord axis of Barilari Bay, Graham Land, west Antarctic Peninsula (65°55′S, 64°43′W). Multi-proxy analytical results constrained by high-resolution geochronological methods (^{210}Pb, radiocarbon, ^{137}Cs) in concert with historical observations capture a record of Holocene paleoenvironmental variability. Our results suggest early and middle Holocene (>7022–2815 cal. [calibrated] yr B.P.) retreated glacial positions and seasonally open marine conditions with increased primary productivity. Climatic cooling increased sea ice coverage and decreased primary productivity during the Neoglacial (2815 to cal. 730 cal. yr B.P.). This climatic cooling culminated with glacial advance to maximum Holocene positions and expansion of a fjord-wide ice shelf during the Little Ice Age (LIA) (ca. 730–82 cal. yr B.P.). Seasonally open marine conditions were achieved and remnant ice shelves decayed within the context of recent rapid regional warming (82 cal. yr B.P. to present). Our findings agree with previously observed late Holocene cooling and glacial advance across the Antarctic Peninsula, suggesting that the LIA was a regionally significant event with few disparities in timing and magnitude. Comparison of the LIA Antarctic Peninsula record to the rest of the Southern Hemisphere demonstrates close synchronicity in the southeast Pacific and southern most Atlantic region but less coherence for the southwest Pacific and Indian Oceans. Comparisons with the Northern Hemisphere demonstrate that the LIA Antarctic Peninsula record was contemporaneous with pre-LIA cooling and sea ice expansion in the North Atlantic–Arctic, suggesting a global reach for these events.

INTRODUCTION

The Antarctic Peninsula (AP) is among the fastest-warming regions on the planet, with atmospheric temperatures rising at a rate of +3.4 °C per century, exceeding five times the global rate (Vaughn et al., 2003). Ice shelf retreat and collapse in the AP—notably documented by the breakup of Larsen Inlet in A.D. 1989 (Skvarca et al., 1999) and of the Prince Gustav Channel and northern Larsen A ice shelves in A.D. 1995 (Rott et al., 1998), and the catastrophic and unprecedented collapse of the Larsen B in A.D. 2002 (Scambos et al., 2003; Domack et al., 2005)—have occurred within the period of recent rapid regional warming, suggesting the southward movement of the –5 °C to –9 °C isotherms, the limit of ice shelf viability (Morris and Vaughn, 2003). Recent removal of ice shelves has facilitated and accelerated grounded ice loss (Scambos et al., 2004; Ferrigno et al., 2008; Berthier et al., 2012). Regionally, 87% of 244 observed glacier fronts in the AP have retreated from historical positions since A.D. 1953 (Cook et al., 2005). Ice shelf collapse and associated ice loss in the AP therefore will contribute to future global sea-level rise as regional and global climatic warming continues (Mercer, 1978; Vaughn et al., 2003; Bentley et al., 2009).

The stability and behavior of ice shelves across the AP varied spatially and temporally during the Holocene (Pudsey and Evans, 2001; Brachfeld et al., 2003; Gilbert and Domack, 2003; Bentley et al., 2005; Hodgson et al., 2006), suggesting a set of complex forcing factors that control the regional climate system. The recent warming trend should be placed in the context of the entire Holocene climate history, specifically with respect to records of ice shelf expansion and collapse. Furthermore, late Holocene records must be documented, specifically millennial- to century-scale climate oscillations (such as the Little Ice Age, LIA), to distinguish the climate events and environmental changes that immediately precede the current regional warming trend and further resolve complexities in the regional and global climate system.

The most recent and severe climate anomaly of the Neoglacial period, the LIA, is classically defined as the period of glacial advance to maximum Holocene positions in the European Alps between A.D. 1550 and 1800 (Lamb,

[†]Current address: Department of Earth & Environment, Boston University, Boston, Massachusetts 02215, USA; achrist@bu.edu.
[§]Current address: College of Marine Science, University of South Florida, St. Petersburg, Florida 33701, USA
[#]CESAM/Department of Geosciences, University of Aveiro, Aveiro 3810-193, Portugal

 doi: 10.1130/B31035.1; 9 figures; 2 tables.

1985; Grove, 1988, 2004). This "event" was initially constrained by the recognition of frontal moraines that stood down-valley of the glacial margins that existed at the time. The LIA was hence named irrespective of the actual climate forcing responsible for the late Holocene readvance of the glaciers. Locally, as in the European Alps, colder, wetter conditions could be linked to the LIA "event," and so this characteristic response was assigned climatic significance. Because the LIA was originally an alpine phenomenon, global extrapolation of this event to glaciated terrains resulted in an asynchronous record, because a multitude of factors besides strict regional temperatures changes can induce a glacial response. For instance, in Southern Patagonia, increased intensity of moisture-bearing westerly winds can induce glacial advance for systems facing the west, despite warming regional temperatures that induce recession for glacial systems with non-westerly aspect (Holmlund and Fuenzalida, 1995). Further, western outlet glaciers of the Northern Patagonian Ice Field are more responsive to changes in precipitation than temperature during the Holocene (Bertrand et al., 2012). Given these issues and chronologic inconsistencies, the global recognition of a "LIA event(s)" has become problematic.

The Antarctic Peninsula (AP) represents an important testing ground for ideas related to the LIA. This is because the region today remains heavily glaciated with a general lack of terrestrially exposed relict moraines. The tidewater character of these glaciers also implies an ice margin dynamic typically considered more complex than that of terrestrially terminating glaciers (Mann, 1986). Most importantly, the AP represents a transitional glacial climate system between temperate, ablation-dominated systems (i.e., Patagonia, South Georgia) and polar systems governed by iceberg calving and ice shelf processes. We proceed by first presenting marine evidence for late Holocene glacial advance, followed by retreat (the classic definition of the LIA from Europe), and then relate these observations to a glacial climate reconstruction that is consistent with facies models for ice shelf and glacio-marine sedimentation. We close by comparing our results to the regional and hemispheric information related to LIA glacial fluctuations, then speculating as to the differences in forcing and timing revealed therein.

THE LIA IN THE ANTARCTIC PENINSULA

South of the polar front in the AP and surrounding sub-Antarctic islands, the available terrestrial glacial and marine sedimentary records indicate glacial advance and climatic cooling broadly during the LIA. On King George Island in the South Shetland Islands, radiocarbon dates of mosses incorporated into Holocene moraines suggest LIA advance of the Collins Ice Cap after 650 cal. (calibrated) yr B.P. (A.D. 1300) (Hall, 2007). Further southeast at James Ross Island in the northeastern AP, a Holocene climate history extracted from an ice core documents a period of late Holocene cooling that supported regional ice shelf expansion beginning at 2500 yr B.P. with a particularly cold span between 800 and 400 yr B.P., but does not indicate a LIA event correlative with the Northern Hemisphere event (Mulvaney et al., 2012). In the eastern AP, apparent exposure ages of glacial erratics indicate expanded ice cover between 600 and 100 yr B.P., suggesting glacial advance and expansion of the Larsen A and Prince Gustav ice shelves during the late Holocene. Radiocarbon and ^{210}Pb activity series (Gilbert and Domack, 2003) and geomagnetic paleointensity chronologies (Brachfeld et al., 2003) of sediment cores collected in the former Larsen A ice shelf area confirm expansion at a maximum age of 700 yr B.P. and minimum age of 400 yr B.P., followed by modern disintegration in A.D. 1995. On Anvers Island in the northwestern Antarctic Peninsula, terrestrial organic matter exposed by recent glacial retreat indicate that the Marr Ice Piedmont was at or landward of present glacial positions 970–700 cal. yr B.P. (A.D. 1050–1250) (Hall et al., 2010).

Late Holocene climate records from sediment cores extracted from the west AP indicate a similar Neoglacial cooling trend and suggest the presence of a LIA climate signature between 700 and 150 yr B.P. (A.D. 1300 and 1850) (Brachfeld et al., 2002; Domack and Ishman, 1993; Domack et al., 1995, 2001; Domack and McClennen, 1996; Leventer et al., 1996, 2002; Shevenell et al., 1996; Harris et al., 1999; Taylor et al., 2001; Warner and Domack, 2002; Milliken et al., 2009; Allen et al., 2010; Hodgson et al., 2013). In Lallemand Fjord, the advance of the Müller Ice Shelf at ca. 400 yr B.P. (ca. A.D. 1600) is recognized as a decline in productivity and an increase in fine-grained siliciclastic sedimentation, but is ultimately inferential with regard to any change in the grounding line position (Domack et al., 1995). While evidence for the LIA climate exists in the west AP, the precise timing of LIA glacial advance and retreat is constrained at only a few sites and is otherwise poorly documented across the region, particularly in glacial marine environments (Bentley et al., 2009).

In this paper we present the first precise chronology of LIA glacial advance and subsequent retreat in Graham Land, west AP. Sediment cores were collected from the entire length of the Barilari Bay during the LARISSA (Larsen Ice Shelf System, Antarctica) cruise in early 2010 aboard the RV/IB *Nathaniel B. Palmer* (NBP10-01). Prior to NBP10-01, Barilari Bay had not been subjected to extensive scientific study. This fjord closes a geographic data gap along the west AP between the Danco Coast (Domack and Ishman, 1993; Domack and McClennen, 1996; Griffith and Anderson, 1989; Harris et al., 1999) and Palmer Deep (Domack et al., 2001; Leventer et al., 2002; Warner and Domack, 2002; Shevenell and Kennett, 2002; Domack et al., 2005) to the north, and Crystal Sound and Lallemand Fjord to the south (Domack et al., 1995, 2003; Domack and McClennan, 1996; Shevenell et al., 1996; Taylor et al., 2001). Unlike Lallemand Fjord and the Danco Coast, Barilari Bay is not geographically protected from the Bellingshausen Sea, and thus, is more susceptible to oceanic influence. Barilari Bay is also situated at a sub-polar latitude, whereas Lallemand Fjord lies fully south of the Antarctic Circle.

STUDY AREA

Barilari Bay (65°55′S, 64°43′W; Fig. 1) was discovered during the first French Antarctic Expedition of 1903–1905 (Charcot, 1905) and re-charted by the British Graham Land Expedition of 1934–1937 (Rymill, 1938). Historic voyages to Barilari Bay recorded seasonally marine conditions since its discovery. Barilari Bay is a re-entrant in the Graham Land coast with the attribute of a fjord system. It is defined by a northwest-southeast–trending fjord 34 km long and 4.8–11 km wide (Figs. 1 and 2). The fjord can be divided into three sections: the glacier-proximal inner fjord, the middle fjord, and more oceanic outer fjord. The inner fjord of Barilari Bay is characterized by the tidewater fronts of the Bilgeri, Weir, Lawrie, and Birley Glaciers. Swath multibeam bathymetric surveys of the inner fjord revealed a prominent grounding zone 5.2 km, 6.3 km, and 4.8 km seaward of the present positions of the Weir, Lawrie, and Birley Glaciers, respectively. The middle fjord is characterized by over-deepened and flatted basins and reaches a depth of 610 m where a zone of at least 35 m of ponded sediment is observed. The outer fjord consists of isolated over-deepened basins (670 m depth) with up to 25 m of ponded sediment, crudely streamlined bedforms including drumlinized and elongated "channel"-appearance bedforms, and crag-and-tail bedforms.

The Otlet, Birley, Lawrie, Weir, and Bilgeri Glaciers and several unnamed glaciers draining the Bruce Plateau terminate into Barilari Bay. A shift toward a general trend of glacial

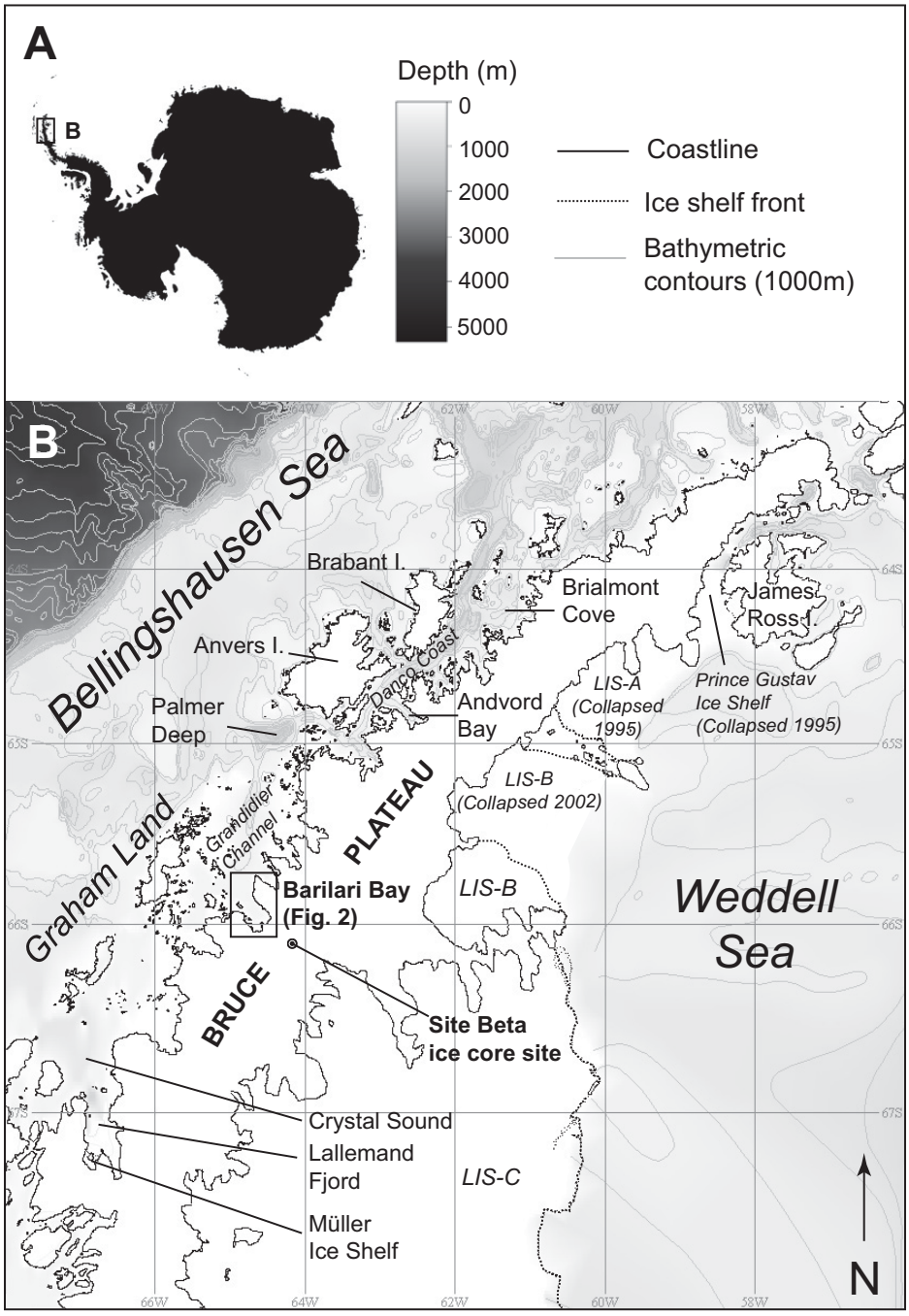

Figure 1. (A) Location of the northern Antarctic Peninsula in Antarctica. (B) North Antarctic Peninsula. Locations with late Holocene records are marked, as well as the location of the Site Beta ice core on the Bruce Plateau.

retreat between 64°S and 66°S in the AP initiated between A.D. 1955 and 1969 (Cook et al., 2005). This 20th-century pattern is expressed in some ice fronts in Barilari Bay by the demise of small, remnant ice shelves since the 1940s and the retreat of the calving fronts of the Birley Glacier and a small unnamed glacier in the inner fjord in the 1960s (Ferrigno et al., 2008). The Bilgeri Glacier, however, experienced a mean ice advance within this time period, although the extent of advance was not delineated by Ferrigno et al. (2008). The other glaciers draining Barilari Bay have maintained ice-front stability since the 1980s (Ferrigno et al., 2008) (Fig. 2). The recent advance and relative stability of ice fronts in this region of the AP versus mean retreat elsewhere suggests accelerated ice discharge from the Bruce Plateau within the past 50 years. Barilari Bay is 12 nautical miles from the ice core recently drilled at Site Beta on the Bruce Plateau by the Byrd Polar Research Center at the Ohio State University (USA) in 2010, providing the most direct comparison between the marine sedimentary and glacial ice records in the Antarctic.

METHODS

Multi-Proxy Analyses

Core Descriptions

Cores KC-54 and KC-55 were opened, described, and sampled soon after collection during NBP10-01. Core JPC-126 was opened, described, and sampled at the Antarctic Research Facility at Florida State University (USA) in 2010. Sediments were described following the procedures established by Kaharoeddin et al. (1988) with the addition of the use of the term "diamicton" following the discussions after Flint et al. (1960).

Particle Size

Grain size was determined using the Malvern Mastersizer/E particle size analyzer and Malvern software suite at Hamilton College (New York, USA). Bulk sediment samples were dispersed in a dispersant solution (sodium hexametaphosphate) and rinsed once. The grain size classification used is: clay (<3.9 μm), fine- and medium-grained silt (3.9–31.00 μm), coarse-grained silt (31.00–62.5 μm), and sand (>62.50 μm) (Wentworth, 1922). This method of sample preparation and data analysis has been utilized successfully in previous similar studies (e.g., Warner and Domack, 2002).

Lamination and Ice-Rafted Debris Indices

X-rays of each core were used to quantify the number of ice-rafted debris (IRD) grains and laminations present within 5 cm intervals of each core. X-ray images for cores KC-55 and JPC-126 were developed at the Korean Polar Research Institute (KOPRI), Republic of Korea, and for core KC-54 at Hamilton College. The IRD index was determined by counting grains greater than 2 mm in size, excluding grains present at the base of turbidite sequences and clasts in diamict. Laminations were defined by sequences bounded using the color contrast in X-ray radiographs.

Bulk Organic Geochemistry

Bulk organic geochemistry was evaluated on acid-washed dried sediment using a Delta Plus Ion ratio mass spectrometer with a COSTECH elemental analyzer. Standards and operating

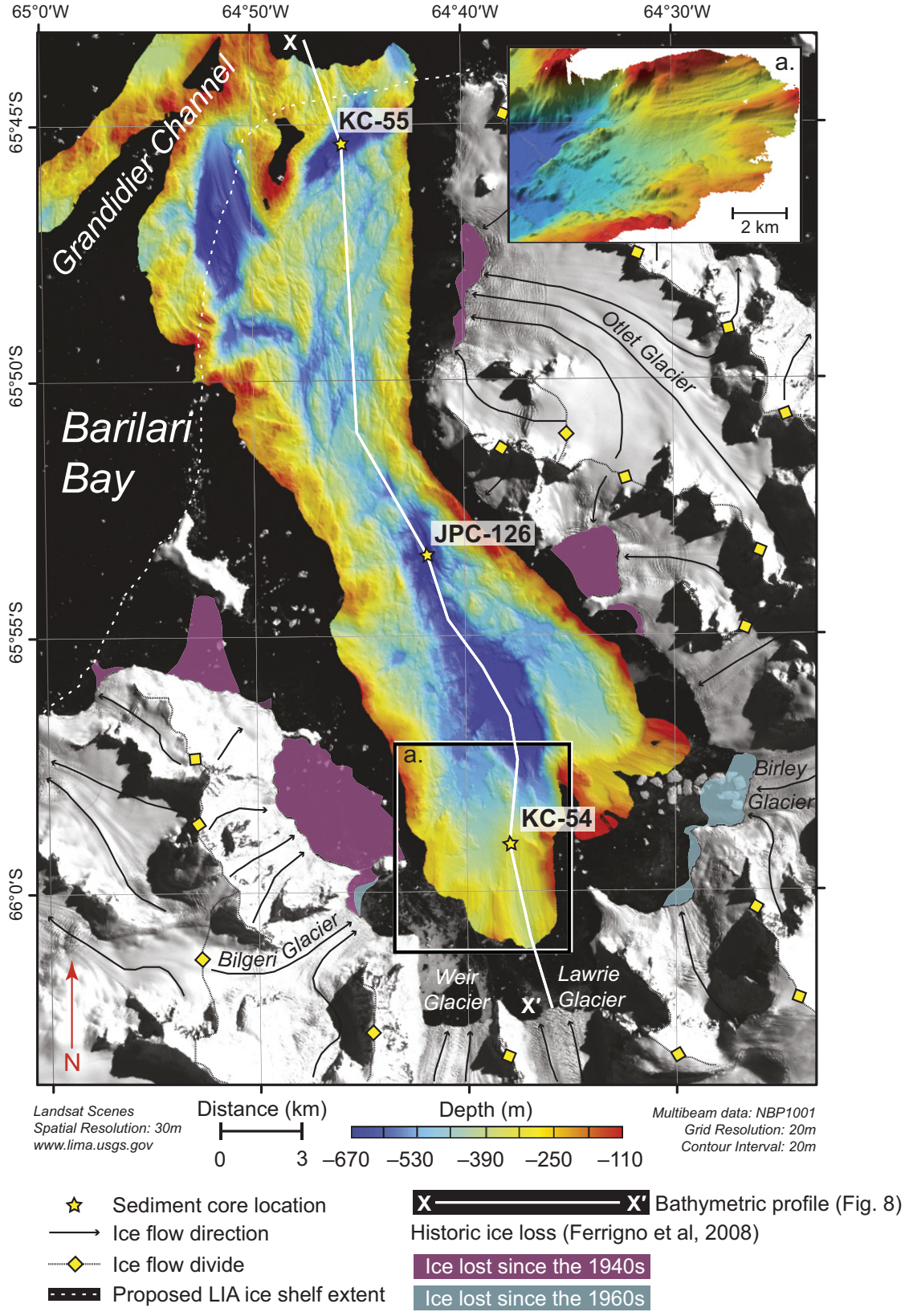

Figure 2. Surface satellite imagery and multibeam swath bathymetry of Barilari Bay. Sediment core locations are marked. Present glacial flow lines and flow divides are indicated. Bathymetric profile line used in Figure 8 is drawn for reference. Historic ice loss is delineated from Ferrigno et al. (2008). Proposed Little Ice Age ice shelf extends to the outer fjord. Inset (a): Oblique view of grounding line and grounding zone wedge in inner Barilari Bay (4× vertical exaggeration).

procedures are provided online (see http://www.hamilton.edu/EMSI). Values of percent total organic carbon (%TOC) and $\delta^{13}C_{org}$ were determined from a suite of analyses, and results were adjusted using standard processing procedures.

Physical Properties

Magnetic susceptibility (MS) was measured for cores KC-54 and KC-55 aboard the *Nathaniel B. Palmer* using a Bartington MS2E surface scanning sensor. MS was measured on split cores for JPC-126 using a Bartington MS2C at the Antarctic Marine Geology Research Facility at Florida State University. MS data were measured at an interval of every centimeter. Water content was measured according to the laboratory procedure at Hamilton College.

Diatoms

Diatom analyses were conducted at Colgate University (New York, USA) and at KOPRI where quantitative diatom slides were prepared following the settling technique described by Scherer (1994). Diatoms were counted along transects at 1000× magnification on a Zeiss Primostar microscope. Where possible, a total of 400 valves were counted, but where diatom abundances were extremely low, a total of 10 transects were counted. Diatom abundances are calculated as millions of valves per gram dry sediment (mvpgs). Relative abundances of the dominant genus, *Chaetoceros*, were calculated based on the total abundance counts described above. However, these data are not calculated or presented for counts where absolute diatom abundances were so low that counting was stopped after 10 transects well prior to counting 400 valves. In these samples, diatom abundances were simply too low for a statistically accurate presentation of the contribution of any species to the total assemblage.

Chronology

Cesium-137 A.D. 1963 "Bomb Spike"

The upper 20 cm of core KC-55 was analyzed to determine the calendar year A.D. 1963 A.D. (47 yr B.P. relative to A.D. 2010) using ^{137}Cs. This method has been previously used in the Antarctic to determine anomalously high ^{137}Cs activity attributed to atmospheric fallout from global nuclear weapons testing (Appleby et al., 1995). Samples were collected at the University of Houston and analyzed at Core Scientific International (Winnipeg, Manitoba, Canada).

Lead-210 Activity Series

The recent chronologies of cores KC-54 and KC-55 were constrained using ^{210}Pb activity series. This method has been used (Gilbert and Domack, 2003) in determining short-term chronologies in marine sediment cores in the Southern Ocean and Antarctic fjords. The sediment-water interface was well preserved in both cores as observed at the time of core splitting, and the water content profiles display a logarithmic decrease down core with a mixed surface layer. Subsamples of sediment were taken at intervals of 1 cm (KC-54) and every other centimeter (KC-55) from the surface to 10 cm (KC-54) and 13 cm (KC-55) depth in anticipation of defining the unsupported ^{210}Pb activity, and at progressively greater intervals to 17 cm (KC-54) and 60 cm (KC-55) depth to determine the supported ^{210}Pb activity. Background levels of supported ^{210}Pb were identified in both cores. By calculating the slope (m) of sample depth versus the natural log of the activity (lnA), one can obtain a linear sedimentation rate (LSR) from $LSR = -\lambda m$, where λ is the ^{210}Pb radioactive decay constant (0.0311 yr^{-1}). Stepped accumulation rates were calculated for both cores based on ^{210}Pb activity, and then each core was assigned a chronology in terms of years before present relative to A.D. 2010.

Radiocarbon Dating

Calcareous foraminifera and some mollusk fragments were used for ^{14}C-radioisotope dating, and samples were sent to the National Ocean Sciences Accelerator Mass Spectrometry (NOSAMS) facility in Woods Hole, Massachusetts (USA). Foraminifera consisted of mostly mono-specific assemblages of clean *Bulimina aculeata* that were in abundance in most intervals within the cores. Results are presented in the text as calibrated ages (cal. yr B.P.) and were calibrated using CALIB ^{14}C calibration program (version 6.0; Stuiver and Reimer, 1993) with the MARINE09 curve (Reimer et al., 2009) (http://calib.qub.ac.uk/calib/). The intervals selected for age determination were chosen based on proximity to unit horizons as well as to interpreted specific sedimentologic events.

Radiocarbon dating in the Southern Ocean is notoriously difficult due to the dominance of upwelling of old deep water derived in large part from the Northern Hemisphere at the Antarctic Divergence (Ingólfsson et al., 1998; Hall, 2009). Deep water is depleted in ^{14}C, and modern marine species that use carbonate from this water typically yield radiocarbon "ages" that are older than 1000 yr (Stuiver et al., 1981; Gordon and Harkness, 1992; Berkman and Forman, 1996). This reservoir effect is not uniform, however, across the Antarctic margin, and regional as well as species-specific disparities (vital fractionations) do occur (Domack, 1992; Domack et al., 2005).

The calibration routine for this study utilized a reservoir correction based on a surface age of 1390 yr B.P. on foraminifera taken from the innermost Barilari Bay core KC-54, from 0 to 3 cm (Table 1). This age is somewhat older than that of living foraminifera observed on the eastern side of the Antarctica Peninsula at 880 ± 45 yr (Domack et al., 2005) and 1040 ± 70 for the nearby Gerlache Strait (Domack, 1992). It is likely that bioturbation has resulted in a slightly older age than the published reservoir ages because the living microfauna would be mixed with deeper, dead microfauna. At present there are no modern ages on living foraminifera within the Graham Land coast region. For these reasons we must assume that the near-surface age of 1390 yr B.P. is a realistic reservoir correction for Barilari Bay. Facies interpretation of each core, the proximity of the surface date, and the fit of the calibration curve to the data points were all considered when choosing the appropriate age model.

RESULTS

Core KC-54

Core KC-54 was collected from the edge of the relict grounding zone in the inner fjord of Barilari Bay at a depth of 341 m, 6.3 km seaward of the calving front of the Lawrie Glacier (Fig. 2), and is 134 cm in length. KC-54 is the most glacial-proximal core. The core was divided into: unit 1 (0–11.5 cm); unit 2, which was subdivided to unit 2a (11.5–38 cm) and unit 2b (38–49 cm); and unit 3 (49–134 cm) (Fig. 3).

Unit 3 (134–49 cm) is a medium to dark gray, structureless, poorly sorted, sandy, homogenous diamicton that extends 90 cm upcore from the core bottom. MS values are highly variable compared to values in overlying units. We do not identify the clasts in unit 3 as IRD. %TOC is at the lowest levels in the entire core (~0.035%), and $\delta^{13}C_{org}$ values are at their most negative, varying between –23.4‰ and –24.5‰. Total diatom abundance is two orders of magnitude lower in unit 3 than in the overlying units, with an average value of 0.055 mvpgs and a maximum value of only 0.223 mvpgs. Total diatom abundance was so low that relative contributions of species to the total assemblage could not be counted with confidence.

At 49 cm there is a sharp contact between unit 3 and unit 2b. Unit 2b (49–39 cm) is a bluish-gray clayey silt. MS values are lower relative to unit 2a and unit 3. IRD content is sparse within unit 2b. There is a limited but notable increase in %TOC and increase of $\delta^{13}C_{org}$ values relative to unit 3. Total diatom abundance increases and ranges between 0.05 and 4.7 mvpgs, and percent *Chaetoceros* averages 81%. While these are signs of a limited increase in upper ocean

TABLE 1. RADIOCARBON CHRONOLOGY

Lab ID	Core number	Depth interval (cm)	Sample material	^{14}C age (yr B.P.)	Age error (yr B.P.)	$\delta^{13}C$	$\Delta^{14}C$	Calibrated age* (cal. yr BP)	Calibrated error*† (cal. yr B.P.)	
									Positive deviation	Negative deviation
OS-86511	KC-54	0–3	Foraminifera	1390	40	–0.60	–165.17	0	0	0
OS-86534	KC-54	38–42	Foraminifera	1600	25	–0.04	–186.73	252	138	137
OS-86510	KC-54	69–75	Shell fragments	7500	45	–0.44	–609.83	7022	146	167
OS-92298	JPC-126	769.5	Complete, undisturbed scaphopod	1770	30	0.76	–202.39	418	78	113
OS-92299	JPC-126	1413	Mollusk fragment	2010	25	–0.13	–226.51	596	69	78
OS-92300	JPC-126	1880	Scaphopod fragments	2180	35	0.80	–242.02	736	131	88
OS-87515	JPC-126	1920	Complete mollusk	2170	25	0.14	–242.78	728	139	90
OS-92187	KC-55	19–24	Foraminifera	1450	45	–0.38	–171.52	82	32	82
OS-92260	KC-55	49–54	Foraminifera	1820	50	–0.35	–208.64	462	42	37
OS-92177	KC-55	80–84	Foraminifera	2050	50	–0.11	–230.93	626	43	60
OS-102267	KC-55	200–205	Foraminifera	3450	45	–0.22	–353.71	2110	64	84
OS-92276	KC-55	250–254	Foraminifera	4030	60	–0.29	–399.09	2815	52	75
OS-92190	KC-55	400–405	Foraminifera	4880	55	–0.20	–459.49	3863	93	73

*Calibrated with Marine09 dataset (Reimer et al., 2009); 1390 yr reservoir age (Barilari Bay, KC-54), Delta R = 990 ± 40.
†One-sigma error.
Note: All sediment cores were collected on cruise NBP 10-01.

biologic activity, eight laminations and no signs of bioturbation were observed in this unit, hence only minimal benthic activity is inferred.

Unit 2b grades into unit 2a (39–11.5 cm), a dark olive gray, sandy silt containing gravel- to cobble-sized IRD grains. We do not classify unit 2a as a diamict, based on the total fewer number of clasts set in a finer-grained matrix observed in the X-ray image and slightly higher water content relative to unit 3. MS values and IRD are increased in unit 2a relative to unit 2b. IRD content increases upcore from 33 grains at the contact with unit 2b to a maximum of 57 grains between 20 and 25 cm depth, and then decreases to 27 grains at the contact with unit 1. %TOC and diatom abundance are relatively low throughout most of unit 2a. Percent *Chaetoceros* shows variability between 68.6% and 90%. Grain size fines upward between 14 and 11.5 cm, and %TOC increases from 0.04% to 0.1%. $\delta^{13}C_{org}$ values increase upcore into unit 1, and range from –22.9‰ to –24.2‰. Diatom total abundance also increases, ranging between 0.1 and 0.5 mvpgs, with only one sample having a higher abundance of 2 mvpgs at 26–27 cm. Few laminations are observed between 10 and 20 cm depth.

At 11.5 cm there is a sharp contact between unit 2 and unit 1 (11.5–0 cm), which consists of water saturated, bioturbated, diatomaceous, light olive gray clayey silt. Between 11.5 and 10 cm there is an interval of gray gravel and cobbles. MS values gradually decrease upcore, corresponding to higher water content, higher diatom abundance, and lower IRD abundance. $\delta^{13}C_{org}$ is more positive relative to unit 2a but decreases from 5 cm to the core top. %TOC increases upcore from ~0.11% at the lower contact at 11.5 cm to ~0.24% near the sediment-water interface. Diatoms are abundant as indicated by the olive color of the sediment, and total diatom abundance increases an order of magnitude upcore, from 2.6 mvpgs at 11.5 cm to a maximum of 23 mvpgs at 3–4 cm. No laminations were observed in this unit. The water content in the upper 15 cm of the core exhibits a logarithmically decreasing downcore trend, indicating that the sediment-water interface was preserved.

Two methods were utilized to establish the chronology for core KC-54: ^{210}Pb activity series and radiocarbon dating. The ^{210}Pb activity series generated an activity profile from which ten ages were calculated. The deepest unsupported ^{210}Pb activity at 13 cm had a calculated age of 98 yr B.P. (A.D. 1912) (Table 1 and Fig. 4). The implied sedimentation rate is 1.33 mm/yr and thus places the bottom of unit 1 (11.5 cm) roughly at A.D. 1925. Three radiocarbon ages were obtained for KC-54: a surface date from

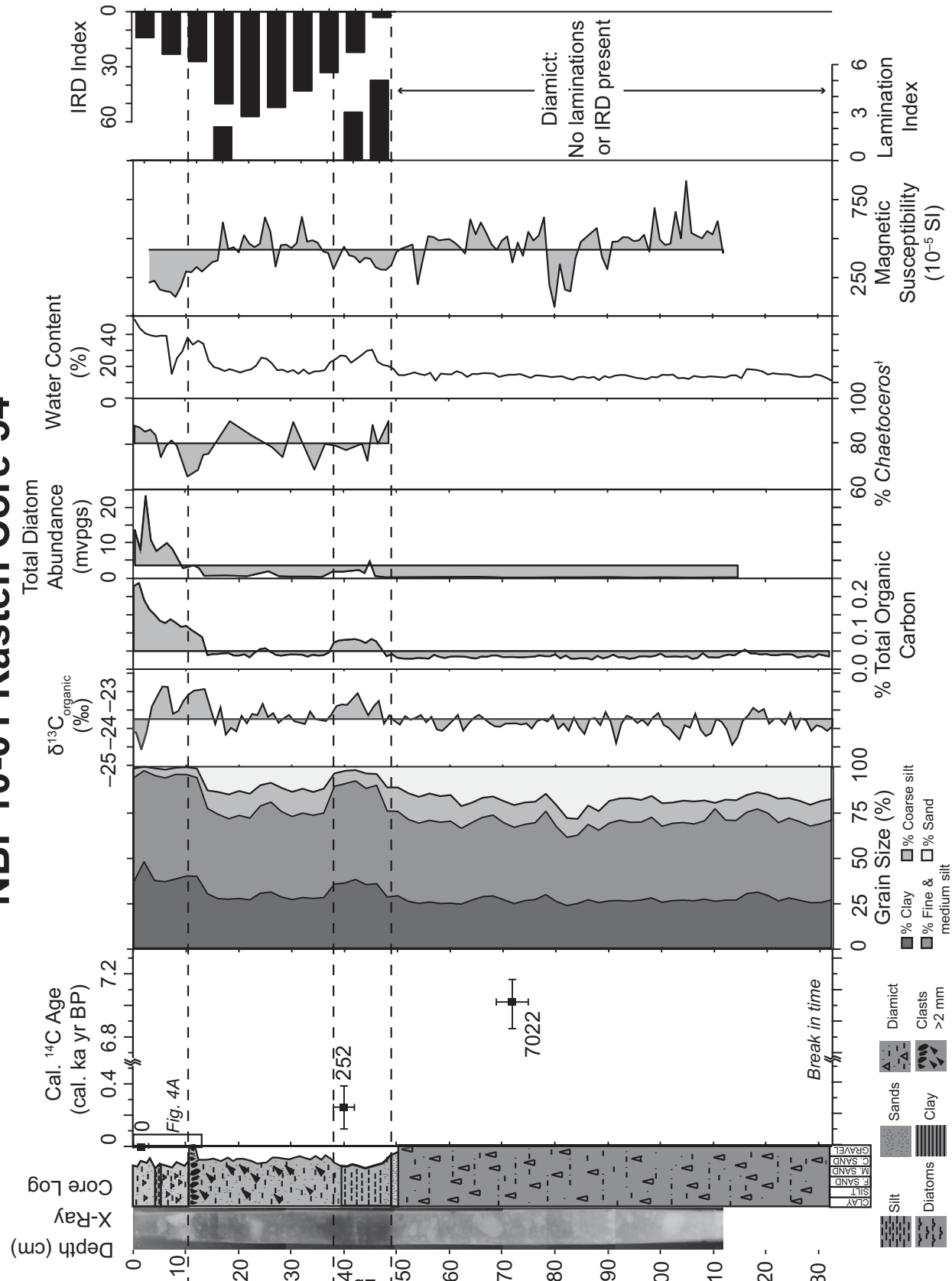

Figure 3. Multi-proxy results and chronology for Kasten Core 54 (KC-54). Multi-proxy results are shaded with respect to the average value for each individual proxy. Note the change in scale for radiocarbon chronology. Interval used in Figure 4 for the short-term chronology assigned by ^{210}Pb activity series is noted. †Due to extremely low total diatom abundances in unit 3, diatom assemblages were not determined (see "Diatoms" section for details). cal.—calibrated; mvpgs—millions of valves per gram dry sediment; IRD—ice-rafted debris.

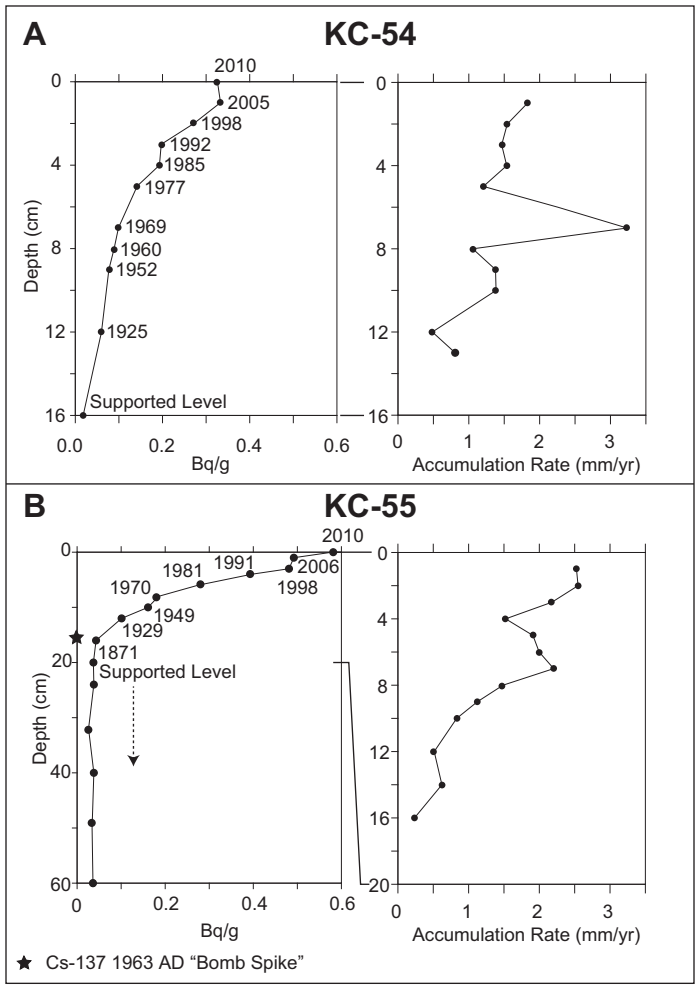

Figure 4. Calculated dates (in A.D.) and sediment accumulation rates from ^{210}Pb activity for cores KC-54 (A) and KC-55 (B). Bq/g is Becquerels per gram of sediment and quantifies the radioactivity of ^{210}Pb in sediment. The ^{137}Cs A.D. 1963 "bomb spike" is shown for KC-55.

foraminifera at 0–3 cm, a date from foraminifera in the laminated silt between 38 and 42 cm (unit 2a-2b contact), and a date from reworked mollusk fragments in unit 3 (69–75 cm). Results are presented in Table 2 and Figure 3.

Core JPC-126

Core JPC-126 is 21.46 m in length and was collected from an isolated basin of ponded sediment ~10 km from the grounding line at a water depth of 642 m (Figs. 2 and 5). The core was divided into three units: unit 1 (0–1.9 m), unit 2 (3.07–18.75 m), and unit 3 (19.10–21.46 m). There are core recovery gaps between each unit attributed to the coring process.

Unit 3 (21.46–19.10 m) consists of olive green diatomaceous, mottled, pebbly sandy silt. MS is lower relative to unit 2 above, reflecting higher diatom content. IRD abundance is enhanced within this interval and reaches a maximum count of 41 grains between 20.47 and 20.52 m. Preserved primary productivity is higher within this unit as indicated by the olive green color and the maximum values of %TOC and $\delta^{13}C_{org}$ of 0.398% and –23.5‰, respectively. Total diatom abundance increases from the core bottom to an average of 72.6 mvpgs, with a maximum value of 222.2 mvpgs at 20.11 m. Percent *Chaetoceros* shows a general decreasing upcore trend.

Following a core recovery gap between 19.10 and 18.85 m, unit 2 (18.75–3.07 m) is a gray laminated silt interbedded with sandy turbidite sequences. Turbidite sequences were recognized by (1) sand and silty sand at the base, which fine upward to clayey silt, (2) peaks in MS that correspond to the sand and silty sand horizons, and (3) overlying silt laminae. Within the laminated intervals, grain size consists of primarily fine and medium silt and sand with little coarse silt and little to no clay. IRD is generally near zero throughout unit 2, with a maximum value of only 4 grains. Productivity within this unit is relatively low, as $\delta^{13}C_{org}$ values and %TOC are depleted and reduced relative to the units above and below. Diatom abundance is low relative to unit 3, with an average of 17.7 mvpgs, and increases to as much as 53.4 mvpgs at 12.005 m.

Following a core recovery gap between 3.07 and 1.9 m, unit 1 (1.9–0 m) is a pebbly, homogenous sandy silt with streaks of green organic-rich silt. MS within this interval is generally lower than that of the rest of the core, reflecting high water content. The most notable characteristic of this unit is the absence of turbidite sequences and marked increase in IRD relative to unit 2. $\delta^{13}C_{org}$ values and %TOC values are increased relative to unit 2 below. Total diatom abundance is similar to that of unit 2 below, at an average of 11.4 mvpgs, but increases to as much as 35.5 mvpgs at 40.5 cm.

Four samples were isolated and prepared for radiocarbon dating in core JPC-126: (1) a complete, undisturbed scaphopod at 7.70 m (unit 2), (2) mollusk fragments at 14.13 m (unit 2), (3) fragments from a single scaphopod at 1880 cm (unit 2), and (4) a complete mollusk at 1920 cm (unit 3) (Table 2 and Fig. 5). There is no radiocarbon age from unit 1. As there is not age control for the top of the core and the sedimentology suggests variable sedimentation rates throughout unit 2, a continuous age model was not developed for JPC-126.

Core KC-55

Core KC-55 was collected from an overdeepened basin in the outer fjord in a water depth of 652 m and is 425 cm in length (Figs. 2 and 6). The logarithmic decrease in water content in the upper 25 cm of the core indicates that the sediment-water interface was well preserved during core extraction. KC-55 can be divided into three units: unit 1 (0–20 cm), unit 2 (20–82 cm), and unit 3 (82–425 cm).

Unit 3 (425–82 cm) is a dark olive green, diatomaceous, pebbly, mottled clayey silt, and displays a general upcore trend of increasing MS and IRD content and decreasing preserved primary productivity. Between 425 and 255 cm, MS and IRD content is decreased below their respective average values for the entire core while %TOC, $\delta^{13}C_{org}$, total diatom abundance, and percent *Chaetoceros* are higher than average. Enhanced biologic activity is evidenced by the maximum %TOC value of 0.89% at 306 cm, total diatom abundance of 1624 mvpgs at 296 cm, and nine burrows observed between 365 and 395 cm. Enhanced preserved productivity is interrupted within this interval of unit 3 by a sandy silt turbidite between 330 and 341 cm,

TABLE 2. LEAD-210 ACTIVITY SERIES CHRONOLOGY

Core number	Sample depth interval (cm)	^{210}Pb activity (Bq/g)	Assigned date (A.D.)	Accumulation rate (mm/yr)
KC-54	0–1	0.326	2010	N/A
KC-54	1–2	0.333	2005	1.83
KC-54	2–3	0.272	1998	1.54
KC-54	3–4	0.197	1992	1.46
KC-54	4–5	0.193	1985	1.54
KC-54	5–6	0.142	1977	1.21
KC-54	6–7	–	1972*	2.26*
KC-54	7–8	0.099	1969	3.23
KC-54	8–9	0.089	1960	1.06
KC-54	9–10	0.077	1952	1.38
KC-54	10–12	–	1945*	1.38*
KC-54	12–13	0.060	1925	0.49
KC-54	13–16	–	1912*	0.81*
KC-54	16–17	0.018	Supported level	†
KC-55	0–1	0.579	2010	N/A
KC-55	1–2	0.492	2006	2.53
KC-55	2–3	–	2002*	2.55*
KC-55	3–4	0.481	1998	2.18
KC-55	4–5	0.396	1991	1.52
KC-55	5–6	–	1986*	1.91*
KC-55	6–7	0.274	1981	2.00
KC-55	7–8	–	1976*	2.20*
KC-55	8–9	0.185	1970	1.49
KC-55	9–10	–	1961*	1.12*
KC-55	10–12	0.161	1949	0.83
KC-55	12–14	0.101	1929	0.51
KC-55	14–16	–	1913*	0.62*
KC-55	16–18	0.043	1871	0.23
KC-55	18–20	–	–	–
KC-55	20–22	0.037	Supported level	†
KC-55	22–24	–	–	–
KC-55	24–25	0.038	Supported level	†
KC-55	25–32	–	–	–
KC-55	32–33	0.026	Supported level	†
KC-55	33–40	–	–	–
KC-55	40–41	0.038	Supported level	†
KC-55	41–50	–	–	–
KC-55	50–51	0.034	Supported level	†
KC-55	51–60	–	–	–
KC-55	60–61	0.036	Supported level	†

Note: Bg/g—Becquerels per gram of sediment. "–" means no sample was analyzed for this depth. N/A—upper-most sample depth; accumulation rate could not be calculated.
*Interpolated value.
†As this sample was at supported level activity, no accumulation rate could be calculated.
Note: All sediment cores were collected on cruise NBP 10-01.

which is marked by a layer of very fine-grained sand that fines upward into a greenish gray silt. Between 255 and 135 cm, MS values are fairly stable but increased relative to values below 225 cm. This depth interval has generally higher IRD content; the maximum IRD abundance, 38 grains, is recorded between 195 and 200 cm. $\delta^{13}C_{org}$, %TOC, total diatom abundance, and percent *Chaetoceros* values decrease below the core average within this interval. Between 135 and 82 cm, grain size fines upward, MS values increase upcore, and IRD is reduced. %TOC decreases from 0.71% to 0.59%, total diatom abundance decreases significantly from 750 to 290 mvpgs, and percent *Chaetoceros* decreases. The decline in organic carbon, however, is paralleled by increased $\delta^{13}C_{org}$ values. These upcore trends in productivity and physical properties continue into unit 2 above.

Unit 3 grades into unit 2 (82–20 cm), a light olive gray, mottled, diatomaceous clayey fine silt. The increase in fine terrigenous sediment is paralleled by an enhanced MS signal above the core average value. IRD is lower in unit 2 relative to unit 3 and unit 1. %TOC decreases from 0.6% at the contact with unit 3 to the core minimum of 0.28% at 38 cm. $\delta^{13}C_{org}$ values are generally less than the average value for the entire core and range between –23.9‰ and –21.9‰. Total diatom abundance decreases significantly within this interval from 291 mvpgs at 82 cm to as little as 58 mvpgs at 21 cm. Percent *Chaetoceros* also decreases below average values in this interval. Within unit 2, the decrease in diatoms is coincident with increased clay content. Laminations were not observed in unit 2.

Unit 2 grades into unit 1 (20–0 cm), a pebbly, mottled, diatomaceous dark olive grayish clayey silt that coarsens upward to a pebbly, mottled, diatomaceous, olive gray silt. MS decreases upcore due to elevated water content. IRD is slightly increased relative to unit 2. %TOC rebounds within unit 1 from 0.3% to 0.6% but does not exceed the core average value. It should be noted, however, that %TOC in core KC-55 is generally an order of magnitude greater than in the other Barilari Bay cores, reflecting its more open, oceanic setting. $\delta^{13}C_{org}$ demonstrates variability with no discernable trend, varying between –22.9‰ at the lower unit contact, –21.9‰ at 14 cm, and –23.5‰ at the sediment-water interface. Total diatom abundance remains decreased at values similar to those of unit 2. This reflects a general upcore trend of decreasing total diatom abundance initiated at 140 cm in unit 3. Percent *Chaetoceros* is variable but is lower than the core average. Laminations were not observed in unit 1.

The chronology of core KC-55 was constrained using the A.D. 1963 cesium "bomb spike" (47 yr B.P. relative to A.D. 2010), ^{210}Pb activity series, and radiocarbon dating. The 1963 Cs bomb spike was determined to be at 15–16 cm, with an inferred sedimentation rate of 3.2–3.4 mm/yr (Fig. 6). ^{210}Pb activity series profiles allowed calculation of 14 dates, the oldest at 139 yr B.P. (A.D. 1871) at 16 cm, with an overall sedimentation rate of 1.21 mm/yr (Table 1 and Fig. 4). Radiocarbon dating complements the above geochronological methods and provides a continuous time series and polynomial age model. Six intervals were selected for foraminifera collection: (1) 19–24 cm (units 1 and 2 contact), (2) 49–54 cm (middle of unit 2), (3) 80–84 cm (units 2 and 3 contact), (4) 200–205 cm (unit 3), (5) 250–254 cm (unit 3), and (6) 400–405 cm (core bottom). Table 2 shows the complete radiocarbon results for KC-55. The six radiocarbon dates from KC-55 represent a continuous sedimentation record for the late Holocene in Barilari Bay (Fig. 6) spanning the last 3863 cal. yr B.P. Depth is converted to age using a third-order polynomial derived from the combined radiocarbon dates and ^{210}Pb activity series from KC-55. Under this age model, the sedimentation rate decreases downcore from 1.19 mm/yr at the surface to 0.033 mm/yr at the core bottom.

DISCUSSION

Seasonally open marine conditions (i.e., seasonally sea ice covered and seasonally open) have been recorded in Barilari Bay since its discovery in the early 20th century (Charcot, 1905; Rymill, 1938), followed by the loss of small remnant ice shelves around the periphery of the fjord since the 1940s, minor glacial retreat since the 1960s, and stable ice front positions at the head of the fjord since the 1980s (Cook et al., 2005; Ferrigno et al., 2008). We propose a sequence of paleoenvironmental variability in Barilari Bay that constrains the glacial and environmental history based on historical observations, the sedimentary record,

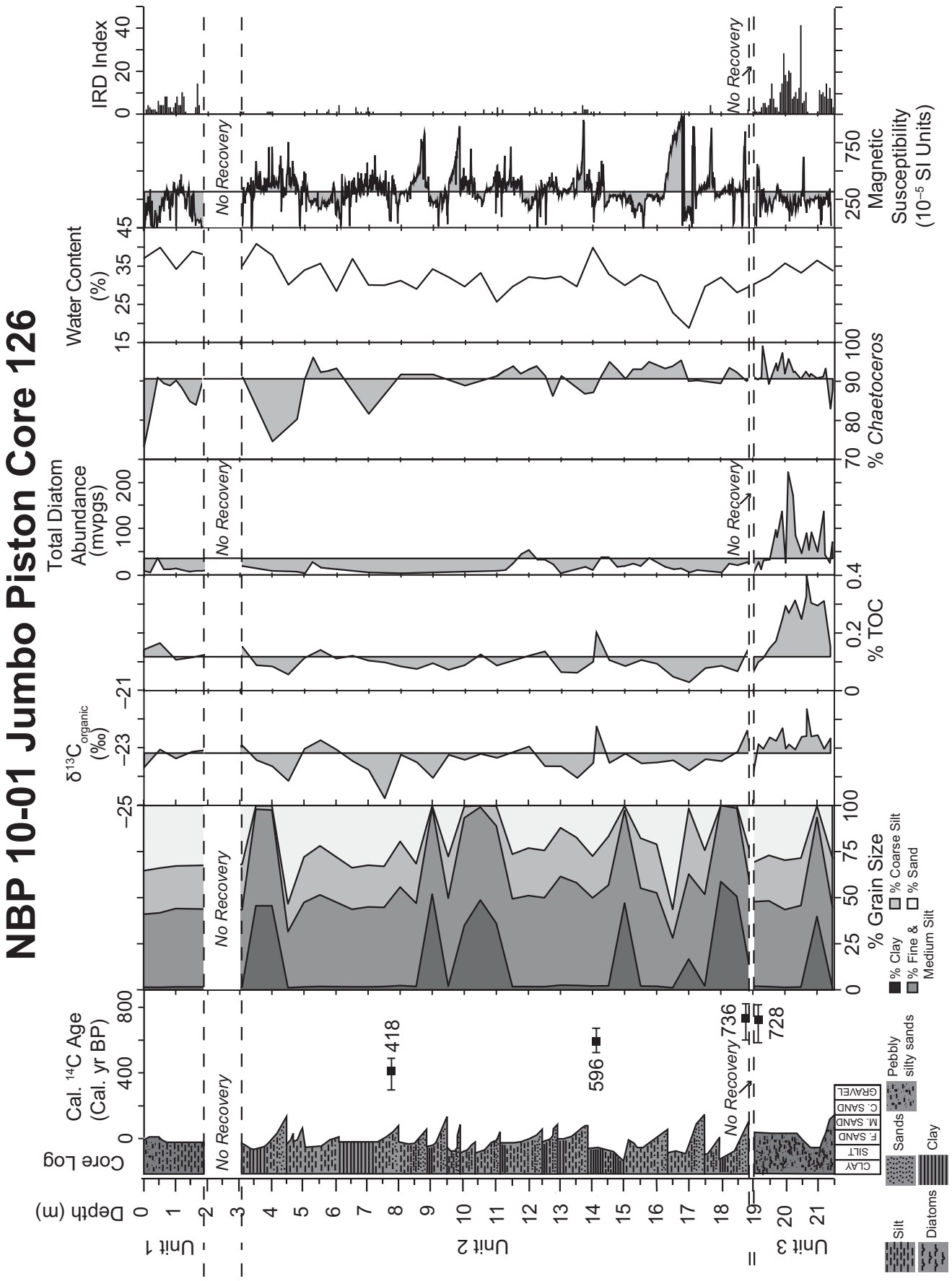

Figure 5. Multi-proxy results and chronology for Jumbo Piston Core 126 (JPC-126). Multi-proxy results are shaded with respect to the average value for each individual proxy. cal.—calibrated; TOC—total organic carbon; mvpgs—millions of valves per gram dry sediment; IRD—ice-rafted debris.

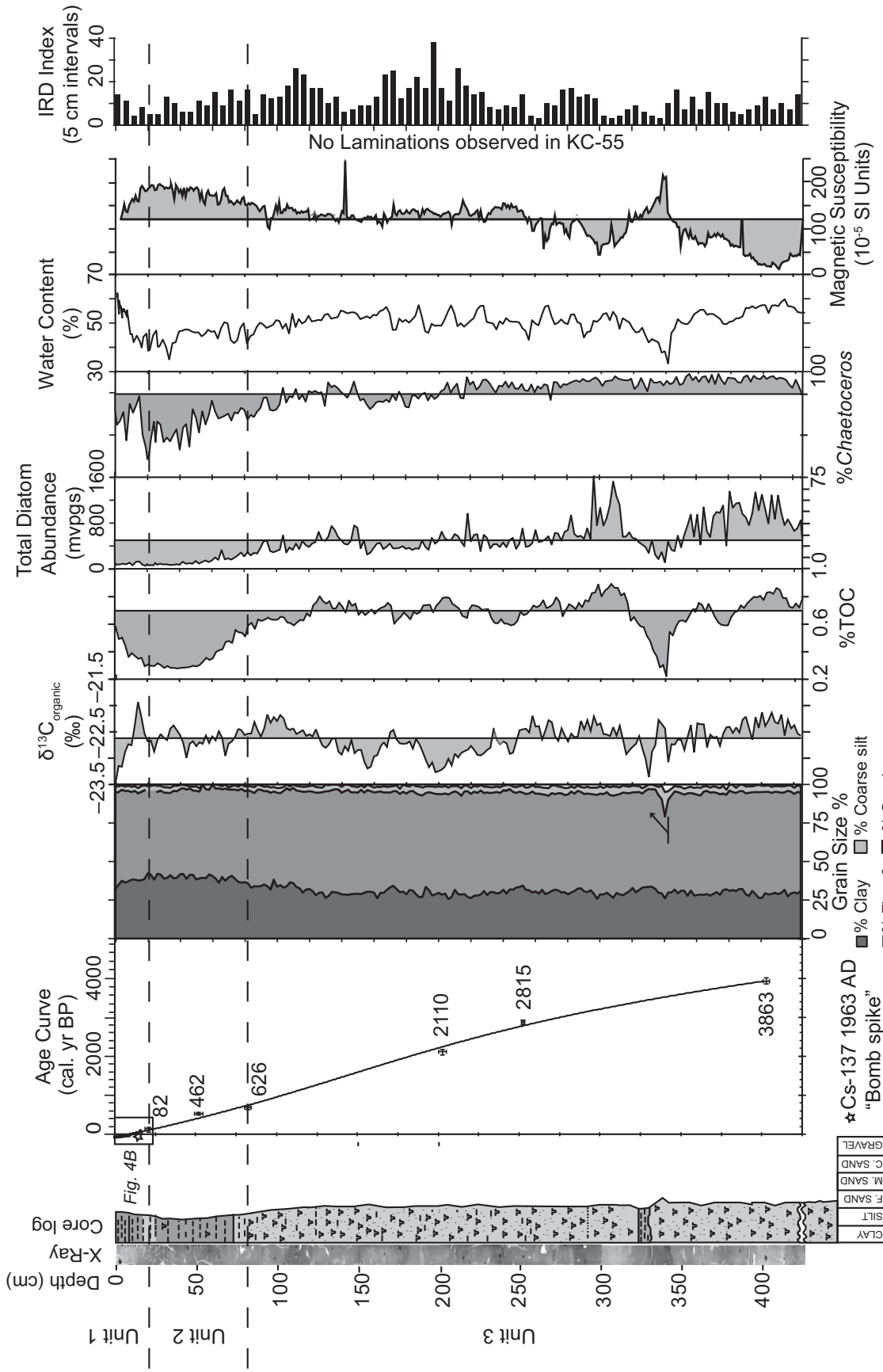

Figure 6. Multi-proxy results and chronology for Kasten Core 55 (KC-55). Multi-proxy results are shaded with respect to the average value for each individual proxy. Interval used in Figure 4 for the short-term chronology assigned by ^{210}Pb activity series is noted. The age model is defined by the equation $y = -5E^{-5}x^3 + 0.0241x^2 + 8.4025x$ ($R^2 = 0.99859$) where x is depth (cm) and y is age (cal. yr B.P.). cal.—calibrated; TOC—total organic carbon; mvpgs—millions of valves per gram dry sediment; IRD—ice-rafted debris.

and a lithofacies model described below. The Holocene paleoenvironmental history of Barilari Bay is summarized in a space-time diagram (Fig. 7) that displays the shifts in environmental setting across the fjord through time.

Lithofacies Model

Sediment lithofacies assigned to the cores within Barilari Bay are based upon decades of information obtained from fjords along the AP. What is unique in this particular setting is that the cores were strategically acquired in position to optimize understanding of the subsurface reflectors and integrated within the multi-beam seafloor morphology. We recognize the following lithofacies: (1) compact, structureless diamicton, (2) laminated silt and clay, (3) graded ensembles of interbedded sand and mud, and (4) diatomaceous mud and diatom-bearing mud with variable content of outsized gravel and pebbles. These lithofacies are interpreted respectively as: (1) sub-glacial till, (2) near–grounding line plume and undermelt deposits, (3) turbidite sediment gravity flow deposits, and (4) hemipelagic and ice-rafted deposits. The facies succession as follows from Walther's Law then allows us to infer changes in depositional environment with constraints upon these various sediments imposed by changing ice shelf cover and glacier extent.

Early and Middle Holocene—Retreated Glacial Positions and Seasonally Open Marine Conditions

Retreated glacial positions during the early Holocene are evidenced by the presence of a mollusk fragment at 69–75 cm depth in core KC-54. The radiocarbon age of this mollusk fragment, 7022 cal. yr B.P. (5072 B.C.), suggests that a younger glacial advance transported

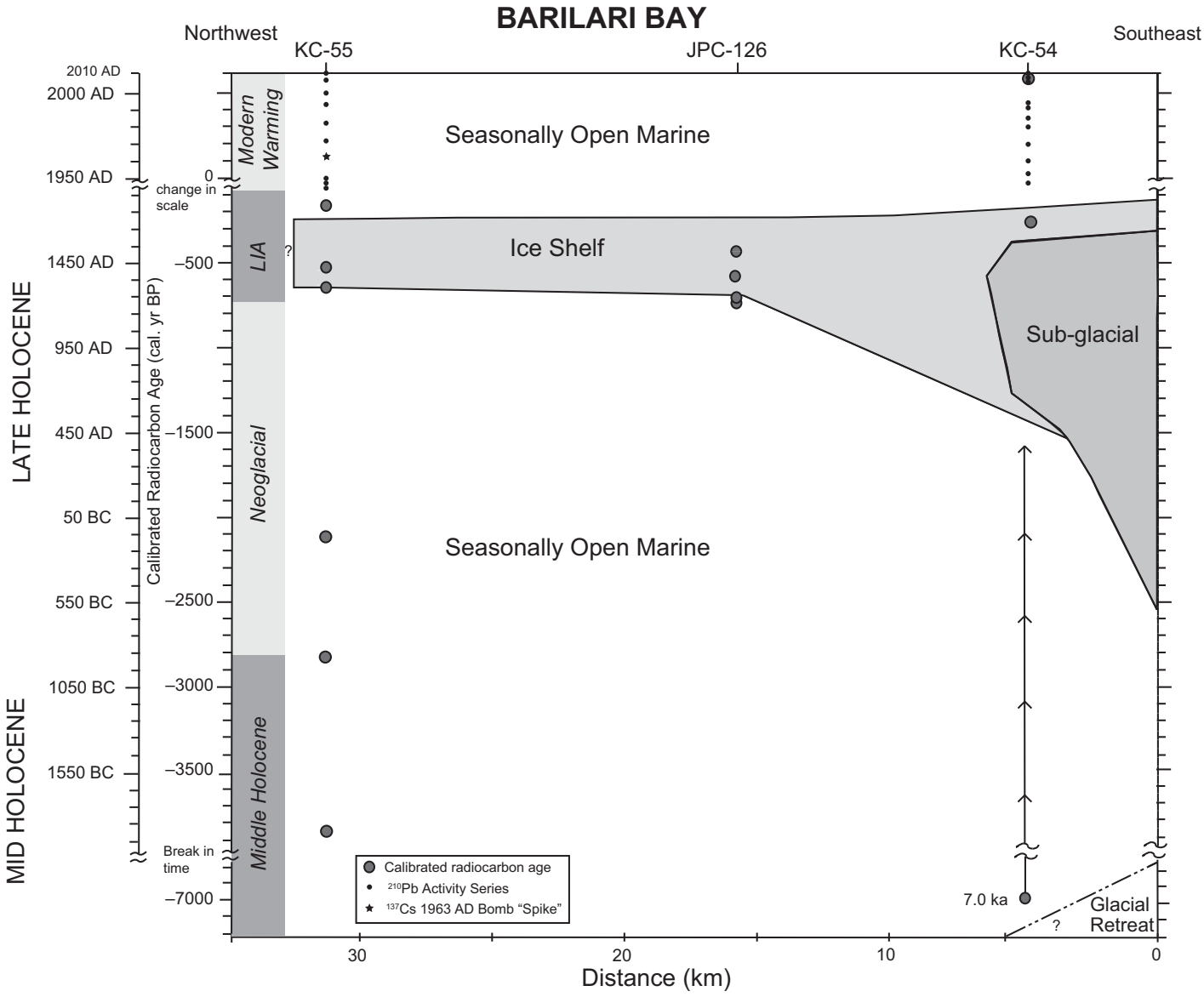

Figure 7. Space-time diagram of late Holocene paleoenvironments and climatic history in Barilari Bay. Location of sediment cores is indicated, along with chronological data for each: calibrated radiocarbon ages (black circles with gray fill), ^{210}Pb activity series (small black dots), and ^{137}Cs A.D. 1963 bomb spike (small black star). Note change of time scale on right at A.D. 1950 and 4000 yr B.P. LIA—Little Ice Age.

and incorporated the mollusk fragments from somewhere further in to the head of the fjord. Similar evidence for retreated glacial positions in the early to middle Holocene is found in shelly tills on Brabant Island (Hansom and Flint, 1989) and organic fragments recently revealed from beneath the ice cap margin on Anvers Island (Hall et al., 2010).

While the chronology of core KC-55 does not constrain the onset of the middle Holocene, the outer fjord record confirms regional observations of enhanced productivity during the middle Holocene (Domack et al., 2001, 2003). Between 3863 and 2815 cal. yr B.P. (1913–865 B.C.), higher %TOC and less-negative $\delta^{13}C_{org}$ relative to the entire KC-55 core indicate greater productivity. Within this interval, total diatom abundance is greater and the assemblage consists primarily of *Chaetoceros* resting spores, considered an indicator of high productivity (Leventer et al., 1996), and thus this interval is interpreted as representing productive seasonally marine conditions. Reduced gravel abundance in unit 3 of KC-55 suggests greater distance from calving ice fronts.

Similar evidence for enhanced productivity during the middle Holocene exists in Neny Fjord, Marguerite Bay (Allen et al., 2010), Lallemand Fjord and Crystal Sound (Domack et al., 1995; Shevenell et al., 1996; Taylor et al., 2001), the Palmer Deep (Brachfeld et al., 2003; Domack et al., 2003), and Maxwell Bay, South Shetland Islands (Milliken et al., 2009). Generally, biological productivity is associated with reduced sea ice coverage and prolonged growing seasons. There is an exception in Maxwell Bay where decreased sea-surface temperature and increased sea ice coverage enhanced productivity (Milliken et al., 2009). Recently, Hodgson et al. (2013) suggested extended middle Holocene regional warming on Horseshoe Island, northern Marguerite Bay, likely related to periods of reduced lacustrine-ice cover that stimulated production.

Neoglacial—Climatic Cooling

At 2815 cal. yr B.P. (865 B.C.), productivity began to decline as reflected in the %TOC, $\delta^{13}C_{org}$, and total diatom abundance proxies in core KC-55 under open marine conditions with greater sea ice coverage. IRD increases upcore in unit 3, suggesting increasing glacial proximity as the calving fronts in Barilari Bay advanced, but seasonally open marine conditions were maintained. In the middle fjord, the late portion of the Neoglacial event is captured in unit 3 of core JPC-126 (>~730 cal. yr B.P.; A.D. 1220), which marks open marine and more productive conditions and the absence of active turbidity currents associated with advanced glacial positions discussed in the "Little Ice Age" section.

The Neoglacial event is observed at a number of sites in the western AP and initiated between 3500–2500 years ago (Domack et al., 2003). Allen et al. (2010) presented a sedimentary record of Neny Fjord in Marguerite Bay where the Neoglacial began ca. 2800 cal. yr B.P. (850 B.C.). Taylor et al. (2001) proposed that the Neoglacial initiated at 2880 cal. yr B.P. (930 B.C.) in Lallemand Fjord, but increased sea ice coverage may have begun as early as 4420 cal. yr B.P. (2470 B.C.). Further north at the Palmer Deep, the Neoglacial began at 3360 cal. yr B.P. (1410 B.C.) and is marked by a decline in productivity and sedimentation rates (Leventer et al., 1996; Domack et al., 2001, 2003). In Maxwell Bay, this period is placed between 2600 yr B.P. and the present, although the sedimentological character shows little evidence of this climatic event (Milliken et al., 2009).

While $\delta^{13}C_{org}$ in the outer fjord of Barilari Bay is enriched between ca. 1325 cal. yr B.P. and 626 cal. yr B.P. (A.D. 625–1324), we do not observe strong evidence for a Medieval Warm Period (MWP) event. Productivity in the outer fjord remains decreased as indicated by decreasing %TOC, total diatom abundance, and percent *Chaetoceros* within this same time interval. The MWP is recognized regionally in the western AP by enhanced productivity in more oceanic settings such as the Palmer Deep and Crystal Sound between 1150–700 yr B.P. (A.D. 850–1300), but is less evident in glacial-proximal environments such as Lallemand Fjord (Domack et al., 2003).

Little Ice Age (LIA)

Glacial Advance and Ice Shelf Development

All three sediment cores provide evidence for climatic cooling and glacial advance with associated development of an ice shelf during the LIA between ca. 730 and 82 cal. yr B.P. (A.D. 1220 and 1868). In the inner fjord, core KC-54 lies at the edge of the fluted grounding zone wedge and captures the maximum Holocene glacial position (Fig. 8A). Unit 3 of KC-54 documents the inner fjord in a sub-glacial environment during the last glacial advance in Barilari Bay. The poorly sorted homogenous diamicton with generally lower water content suggests deposition from sub-glacial processes. Very low %TOC and total diatom abundance and highly negative $\delta^{13}C_{org}$ indicate lower primary productivity caused by light limitation and other biologic activity.

Glacial advance in Barilari Bay altered sedimentological processes across the entire fjord. In core JPC-126, the transition to the LIA is recognized at ca. 730 cal. yr B.P. (A.D. 1220) by a shift to gray laminated silt with interbedded sandy turbidite sequences (unit 2) deposited as glaciers advanced to the edge of the grounding line. At these advanced positions, meltwater pulsing along the grounding line ejected sediment plumes into the fjord, depositing laminated silts and clays. Fluctuations of the ice margin at this advanced position caused portions of the edge of the grounding zone wedge to collapse, and turbidity currents carried sediment through channels toward the zone of ponded sediment in the middle fjord. Both of these depositional processes likely increased sedimentation rates within the middle fjord relative to seasonally open marine conditions.

The decay of remnant ice shelves demonstrated in historic records and our sedimentological evidence suggests that a prehistoric ice shelf expanded across Barilari Bay during the LIA. This environment is marked by both low IRD abundance and decreased productivity within this time interval. In the presence of the ice shelf, and thus absence of iceberg calving processes, entrained glacial debris is not rafted from the ice margin and deposited across the fjord. Sub–ice shelf conditions precluded primary productivity as expressed in the decreased %TOC, more-negative $\delta^{13}C_{org}$ values, reduced total diatom abundance, and fewer *Chaetoceros* within this interval. However, enhanced sedimentation rates under the advanced glacial position may partially mask biogenic sedimentation in this interval and region of the fjord. An open marine influence was maintained near the ice shelf margin as diatoms were likely transported under the ice shelf by wind-driven surface currents.

In the outer fjord of Barilari Bay, the LIA is captured between 626 and 82 cal. yr B.P. (A.D. 1324–1868) in unit 2 of core KC-55, which is marked by a fining of grain size and decreased primary productivity. The fining in grain size and increasing upcore trend in MS reflects increased fine-grained siliciclastic sedimentation, preservation instead of dissolution of fine-grained magnetite in the zone of low %TOC, and reduction in biogenic input from diatoms. The negative shift in $\delta^{13}C_{org}$, and decrease in %TOC, total diatom abundance, and percent *Chaetoceros*, are attributed to the expansion of the ice shelf into or near the outer fjord and more pervasive sea ice coverage. This reduction in productivity and fining of particle size is comparable to trends observed in Lallemand Fjord when the Müller Ice Shelf expanded during the LIA 400 yr B.P. (Domack et al., 1995; Shevenell et al., 1996). Given the olive gray color, diatomaceous nature of the sediment, and %TOC values that are an order of magnitude greater than in the middle

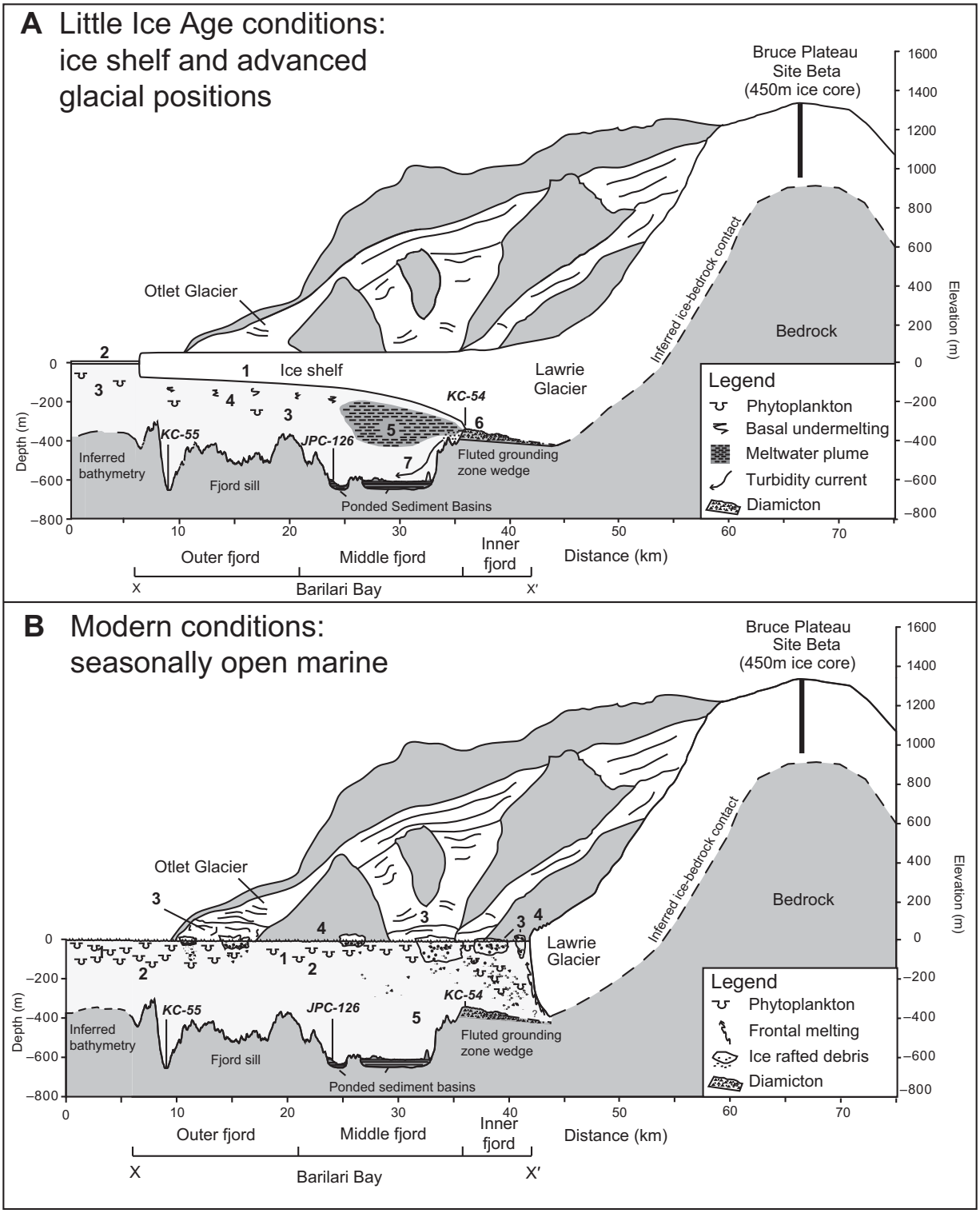

Figure 8. Schematic diagram of Barilari Bay. The bathymetric profile traced along the fjord axis in A and B can be found in Figure 2. Cross-section view is looking to the northeast. Numbers refer to environmental and sedimentological processes active during this each climate event. (A) Little Ice Age conditions: 1—fjord-wide ice shelf; 2—increased sea ice coverage and fast ice; 3—decreased primary productivity; 4—reduced basal melting of the ice shelf; 5—ejection of meltwater plumes of fine-grained siliciclastic sediment; 6—glacial advance to maximum Holocene positions over a fluted grounding zone wedge; 7—turbidity currents emanating from the grounding line. (B) Modern seasonally marine conditions in Barilari Bay: 1—seasonally open marine conditions; 2—increased primary productivity; 3—increased iceberg calving and ice-rafted debris deposition; 4—re-treated glacial positions with frontal melting at the calving fronts; 5—absence of turbidity currents and meltwater plumes.

and inner fjord in this interval, proximity to the ice shelf front and seasonally marine conditions, albeit with greater sea ice coverage, must have been maintained. A bathymetric rise northeast of the mouth of the fjord may have served as a pinning point for the expanded ice shelf. Under this scenario, IRD in unit 2 of KC-55 may have been sourced from the grounding line of the advanced Otlet Glacier, where basal melt-out could have supplied IRD grains.

The precipitation accumulation zone and rate must have increased to allow glacial advance, and the ablation zone and rate must have decreased for the ice shelf to expand. Further south on the AP (75°55′S, 84°15′W), the ice core from Siple Station records relatively warmer conditions and decadal-scale periods of increased snow accumulation rate, possibly due to intensification of the Southern Westerlies between A.D. 1500 and 1900 (Mosley-Thompson et al., 1990). While increased snow accumulation could have caused a positive shift in the mass balance for western AP glaciers, higher temperatures contradict the expansion of an ice shelf in Barilari Bay, as it implies that the –5 to –9 °C isotherm did not migrate north during the LIA. We propose, therefore, a shift in oceanographic conditions that decreased frontal melting and undermelting of glacier fronts, allowing the expansion of the Barilari Bay ice shelf. Reduced upwelling of warm, saline circumpolar deep water (CDW) during the LIA interval may have permitted the formation of the ice shelf in Barilari Bay. The advance of the Müller Ice Shelf at 400 yr B.P. (Domack et al., 1995) further south in Lallemand Fjord suggests a regional climatic shift that encouraged ice shelf growth during the LIA and has also been attributed to decreased presence of CDW.

Ice Shelf Recession and Glacial Retreat

At the edge of the grounding zone in core KC-54, the sharp contact between diamict (unit 3) and laminated clayey silt (unit 2b) marks initial glacial retreat. The appearance of IRD, fining in grain size, and decrease in MS values relative to unit 3 indicate a transition from sub-glacial deposition to pelagic sedimentation. Laminations suggest deposition related to meltwater pulsing near the grounding zone. The limited increase in %TOC and $\delta^{13}C_{org}$ reflects continued low primary productivity under sub–ice shelf conditions. Reduced biologic activity is also evidenced by the bluish gray color of the unit, low abundance of microfossils, and preservation of laminations that would otherwise be disturbed by bioturbation under more productive conditions. Unit 2b was deposited in proximity to grounded ice, but some distance from the calving front of the ice shelf; thus the transition between units 3 and 2b represents an ice "back-off" event from the edge of the grounding line and occurred sometime prior to 252 ± 137.5 cal. yr B.P. (A.D. 1698). This suggests that the maximum extent of ice advance during the LIA occurred in the first half of the LIA (730 to >252 cal. yr B.P.; A.D. 1220 to >1698) followed by slow, gradual retreat until 82 cal. yr B.P. (A.D. 1868).

The demise of the LIA ice shelf in Barilari Bay may be analogous to recent observations below the ice shelf extending from the Pine Island Glacier in West Antarctica, where an ice "back-off" event was observed at Pine Island Glacier in the late 1970s (Jenkins et al., 2010). Jenkins et al. (2010) suggested that although the ridge feature along the edge of the grounding line initially impeded influx of warm, saline CDW to the base of the glacier, thinning of the ice shelf from above by increased atmospheric temperatures and from below by CDW enlarged the cavity between the edge of the grounding line and glacier base, ultimately increasing and accelerating ice retreat. While the ice shelf in Barilari Bay may have receded in a similar fashion, the timing of the initial ice "back-off" event some time prior to 252 cal. yr B.P. suggests that ice recession in this study area was much more gradual.

Unit 2a in core KC-54 signifies that the complete transition from sub–ice shelf to open marine conditions in the inner fjord occurred between 252 ± 137.5 cal. yr B.P. (A.D. 1698) and 98 yr B.P. (A.D. 1912). Although the first French Antarctic Expedition recorded seasonally open marine conditions in Barilari Bay between A.D. 1903 and 1905, expedition records are not specific regarding conditions in the inner fjord (Charcot, 1905). The charts produced by the British Graham Land Expedition, however, explicitly record seasonally open marine conditions in Barilari Bay between A.D. 1934 and 1937 (Rymill, 1938). Grain size gradually coarsens upwards, with enhanced IRD deposition indicating increasing input of terrigenous sediment as entrained debris fell out of the receding ice shelf, similar to observations at the former Prince Gustav Channel and Larsen A ice shelves (Gilbert and Domack, 2003). The increased flux of terrigenous sediment into the inner fjord masked the input of biologic components as shown by the decreased %TOC. The maximum number of IRD grains occurring between 20 and 25 cm marks the point in time when the calving front was most proximal to the KC-54 collection site. Above 20 cm, IRD abundance and MS values decrease, followed by significantly increased productivity proxies indicating that the calving front retreated landward toward its present position, affording more open marine conditions at the site.

Modern Warming

Unit 1 in core KC-54 represents the modern open marine conditions that facilitate primary productivity as indicated by maxima in %TOC and $\delta^{13}C_{org}$. Benthic activity is indirectly documented by bioturbation. IRD and MS decrease upcore, marking greater distance from the core collection site to, and less terrigenous sediment input from, the glacier fronts. The horizon of cobbles and gravel at 10 cm is interpreted as an ice rafting event where the calving front was landward of the KC-54 collection site. The reduced flux of terrigenous sediment also enhances the biologic signal preserved in unit 1. Figure 8B illustrates Barilari Bay under seasonally open marine conditions.

In the middle fjord, the transition from sub–ice shelf to seasonally open marine conditions occurs between unit 2 and unit 1 in JPC-126. Due the core recovery gap that exists between 1.87 and 3.07 m, the exact timing of this climatic shift is not constrained in the middle fjord. Unit 1 of core JPC-126, however, indicates an environmental shift toward open marine conditions. The most notable changes are the absence of sandy turbidite sequences and presence of IRD relative to unit 2. As glacial positions retreated, the ice margin no longer stood at the edge of the grounding zone. As a result, meltwater pulsing along the grounding line ceased along with slope instability and associated turbidity currents. Glacial retreat and the gradual demise of the ice shelf also increased calving events and consequently IRD deposition. Interestingly, total diatom abundance and percent *Chaetoceros* do not rebound in the upper unit; however, the sediment-water interface, and thus possibly the transition to more productive open water conditions, was not well preserved in JPC-126.

In the outer fjord, ice shelf recession and glacial retreat was completed by 82 cal. yr B.P. (A.D. 1868), and the modern seasonally open marine conditions are represented by unit 1 in KC-55. This environmental shift toward seasonally open marine conditions is expressed by a rebound in productivity and coarsening of grain size upcore, with a related reduced MS signal. Total diatom abundance continues to decrease upcore in unit 1 however, despite an increase in %TOC. This suggests that primary productivity increased as a consequence of increased abundance of groups other than diatoms—presumably a soft-bodied algae, perhaps cryptophytes, as have been observed to be associated

with increased glacial meltwater and lower sea surface salinities (Moline et al., 2004). The variability in $\delta^{13}C_{org}$ may further reflect oceanographic changes that may have affected the local biological community.

Comparison with Late Holocene Glacial Records in the Southern Hemisphere

The timing and magnitude of LIA glacial advance in Barilari Bay corresponds to regional enhanced climatic cooling and glacial advance in the AP, but the LIA is asynchronous with glacial records from elsewhere in the Southern Hemisphere. Compiled late Holocene glacial records from middle to high latitudes in the Southern Hemisphere are presented in Figure 9. The following chronology summary will be discussed in terms of calendar years (B.C./A.D.) where possible, or in terms originally used by the authors where conversion to calendar years was not possible.

South of the polar front and across both the western and eastern AP, the Barilari Bay record confirms a tightly constrained period of glacial advance between A.D. 1200 and 1400. Glacial advance in Barilari Bay is broadly coincident with the advance of the Müller Ice Shelf at ca. A.D. 1600 (Domack et al., 1995), and regional cooling and decreased productivity across the western AP between A.D. 1300 and 1850 (Domack et al., 2003). The terrestrial glacial record on Anvers Island is also in agreement, as the Marr Ice Piedmont advanced sometime after A.D. 1250 (Hall et al., 2010). The Barilari Bay record corresponds to the glacial advance in the eastern AP where both terrestrial (Balco et al., 2013) and glacial marine (Gilbert and Domack, 2003; Brachfeld et al., 2003) evidence indicates late Holocene glacial advance and re-establishment of the Prince Gustav Channel and Larsen A ice shelves between A.D. 1300 and 1600. The Collins Ice Cap on King George Island in the South Shetland Islands advanced at A.D. 1300 (Hall, 2007). Late Holocene glacial advances in the AP and the South Shetland Islands coincide with two periods (A.D. 1275–1300 and A.D. 1430–1455) of abrupt and intensified cooling and sea ice growth around Iceland and Arctic Canada, attributed to volcanic forcing (Miller et al., 2012), but predate the classically defined period of LIA alpine glacial advance in the European Alps (Lamb, 1985).

North of the polar front on South Georgia, a late Holocene advance occurred at A.D. 900 and predates glacial advance in the AP and South Shetlands (Clapperton et al., 1989; Bentley et al., 2007). This advance was during a period of relatively warmer conditions and reduced ice extent in the western AP (Domack et al. 2003). Glacial advance on South Georgia is attributed to increased precipitation afforded by southern excursion of the Southern Westerlies, warmer temperatures, and reduced sea ice conditions, leading to the anti-phase relationship with AP glacial records (Bentley et al., 2007). Glaciers in the Kerguelen Islands in the southern Indian Ocean were at maximum Holocene positions in the late 19th century (Frenot et al., 1993).

In southern South America, there is general synchronicity with the AP for glacial advance between A.D. 1200 and 1400, but the records later diverge, as additional pulses of glacial advance are observed during the classically defined LIA period. In Tierra del Fuego, the Ema Glacier advanced in sync with AP glaciers at 695 ^{14}C yr B.P. but then readvanced between 379 ^{14}C yr B.P. and 60 yr B.P. (Strelin et al., 2008). In the Gran Campo Nevado (Chile), Glaciar Lengua advanced to maximum Holocene positions between A.D. 1280 and 1460, followed by overall retreat and six smaller, punctuated advances between A.D. 1628 and 1941 (Koch and Kilian, 2005). Further north in the Monte Fitz Roy region (Argentina), glaciers reached maximum LIA positions later, in the A.D. late 1500s to early 1600s (Masiokas et al., 2009). In the Southern Patagonian Ice Field and Northern Patagonian Ice Field, LIA glacial advance ages range from A.D. 1220 to 1890, but a majority of Southern Patagonian Ice Field glaciers advanced after A.D. 1600 (Glasser et al., 2004). Most of the outlet glaciers in the Northern Patagonian Ice Field advanced later, between A.D. 1650 and 1766, and retreated from their maximum late Holocene positions between A.D. 1860 and 1870 (Harrison et al., 2007). In the northern sector of the Northern Patagonian Ice Field, the Gualas Glacier advanced to maximum Holocene positions between 2230 B.C. and A.D. 1100, and experienced three smaller advances between A.D. 1790 and 1940 (Bertrand et al., 2012).

In New Zealand, late Holocene glacial advance occurred out of sync with the AP and southern South America and at the end of the classic LIA time period. On the western side of the divide of the Southern Alps, the Strauchon Glacier advanced prior to the AP and southern South America glaciers at 390 B.C., A.D. 310, and A.D. 910 (Winkler, 2009). The Franz Josef Glacier, however, advanced during the classic LIA time frame, with the most extensive advance some time before A.D. 1600 and smaller advances at A.D. 1600 and A.D. 1800 (McKinzey et al., 2004). On the eastern side of the Southern Alps, glaciers advanced to maximum positions in the early and middle Holocene. Late Holocene glacial advance on the eastern side of the Southern Alps occurred slightly later than in the AP and southern South America. The Mount Cook glaciers advanced at A.D. 1440 (Schaefer et al., 2009), and the Cameron Glacier advanced at A.D. 1362 and A.D. 1492, followed by smaller advances after A.D. 1770 (Putnam et al., 2012). On the North Island, Mount Taranaki glaciers retreated after A.D. 1500 (Brook et al., 2011). The asynchronous behavior of New Zealand glaciers during the classic LIA has been attributed to a shift to a negative phase of the Interdecadal Pacific Oscillation (Schaefer et al., 2009) and the southern migration of the Intertropical Convergence Zone (Putnam et al., 2012), both of which bring warmer and drier conditions to New Zealand.

The timing of LIA glacial advances is increasingly younger to the north from the AP toward the Northern Patagonian Ice Field, indicating that the LIA was not a synchronous event across the southeast Pacific sector. This chronological progression may be in response to northward migration of the Southern Westerlies, which control storm tracks, regional precipitation, cloud cover, and temperature patterns that influence local glacial behavior (Holmlund and Fuenzalida, 1995; Bertrand et al., 2012). Alternatively, the overall pattern may reflect the response time of the glacial system under a uniform climatic shift. If climatic episodes appropriate to induce glacier growth take place across the entire region (Patagonia to AP) and are of limited duration, then asynchronous response may simply indicate the lag time for colder and more sluggish systems (i.e., those in the AP). If the forcing factor is of long enough duration, then a delayed response across the region should reflect the varying response times across glacial dynamic boundaries. We suggest that the AP glaciers indeed may be sluggish, as their calving lines are not as easily stabilized by sediment provisioning in deep water, and fast ice to ice shelf transitions may take several decades, under a generally colder climate. Indeed, sediment delivery rates are higher and ice flow dynamics are greater for Patagonian glaciers than their counterparts in the AP (Boldt et al., 2013).

CONCLUSIONS

Based on our observations and the historical record, we propose this high-resolution chronology of paleoenvironmental history in Barilari Bay (Fig. 7):

1. Early Holocene and middle Holocene (>2815 cal. yr B.P.; >865 B.C.) retreated glacial positions and seasonally open marine conditions with enhanced primary productivity;

2. Neoglacial (2815 to ca. 730 cal. yr B.P.; 865 B.C. to A.D. 1220) seasonally open marine conditions with increased sea ice coverage—

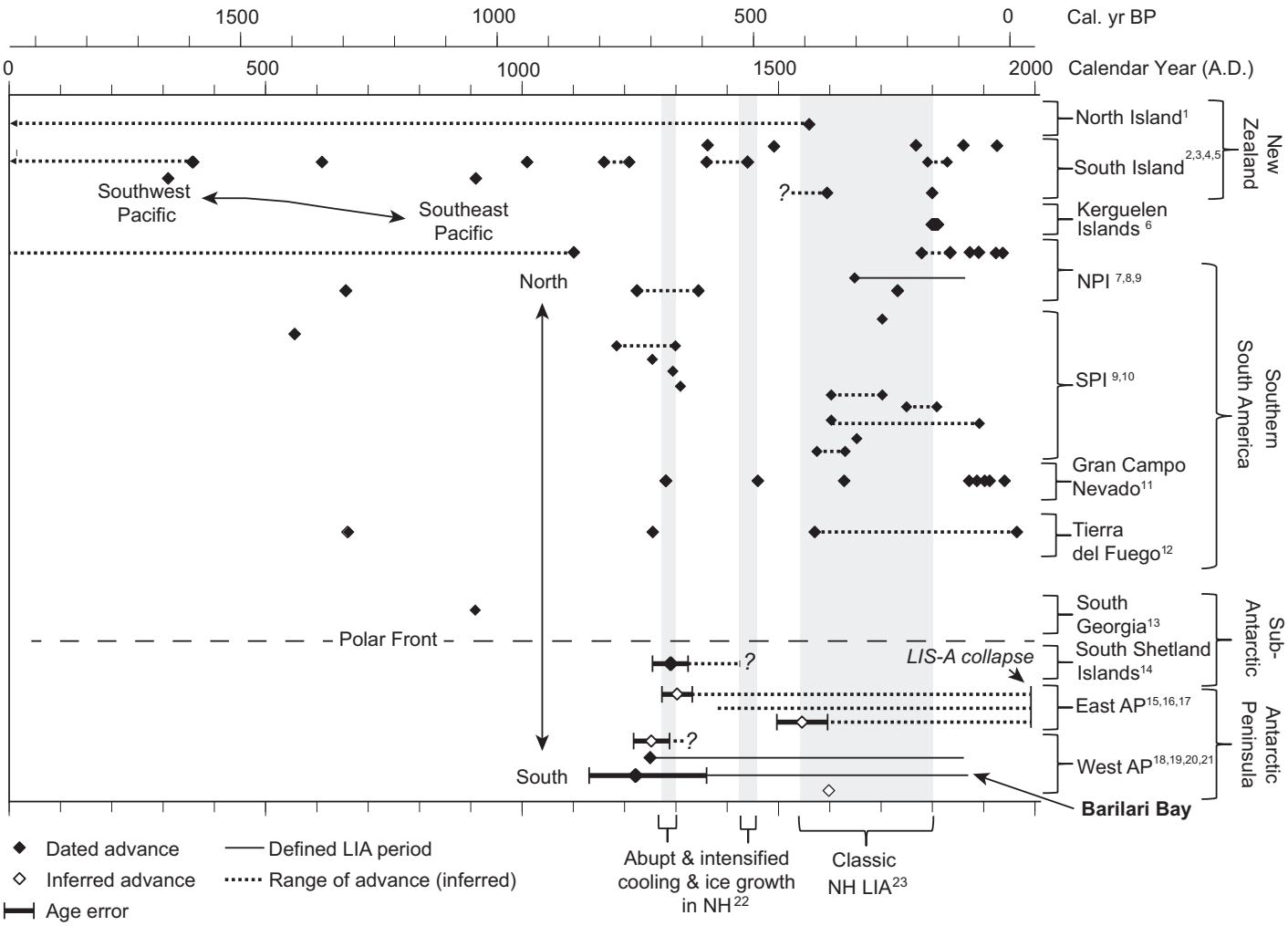

Figure 9. Late Holocene glacial advance and defined Little Ice Age (LIA) glacial intervals in the Southern Hemisphere. Cal.—calibrated; NPI—Northern Patagonian Ice Field; SPI—Southern Patagonian Ice Field; AP—Antarctic Peninsula; NH—Northern Hemisphere; LIS-A—Larsen Ice Shelf A. Black diamonds indicate dated glacial deposits. Hollow black diamonds indicate inferred ages of glacial advance. Black diamonds with dotted lines between them bracket possible advance age ranges. Solid black line indicates defined LIA glacial period. Age error bars are included for AP records where appropriate. Periods of abrupt (A.D. 1275–1300) and intensified (A.D. 1430–1455) cooling and ice growth in Iceland and Arctic Canada attributed to volcanic forcing (Miller et al., 2012) are shaded in gray, as is the classic Northern Hemisphere LIA (A.D. 1550–1800). Superscripts refer to the following references: [1]Brook et al., 2004; [2]Putnam et al., 2012; [3]Schaefer et al., 2009; [4]Winkler, 2009; [5]McKinzey et al. 2004; [6]Frenot et al., 1993; [7]Bertrand et al., 2012; [8]Harrison et al., 2007; [9]Glasser et al., 2004; [10]Masiokas et al., 2009; [11]Koch and Kilian, 2005; [12]Strelin et al., 2008; [13]Bentley et al., 2007; [14]Hall, 2007; [15]Gilbert and Domack, 2003; [16]Balco et al., 2013; [17]Brachfeld et al., 2003; [18]Hall et al., 2010; [19]Domack et al., 2003; [20]This study (Barilari Bay); [21]Domack et al., 1995; [22]Miller et al., 2012; [23]Lamb, 1985.

we do not observe strong evidence for a MWP event in Barilari Bay;

3. Little Ice Age (ca. 730–82 cal. yr B.P.; A.D. 1220–1868) glacial advance to maximum Holocene positions and development of a fjord-wide ice shelf—prehistoric glacial retreat and gradual recession of the ice shelf initiated some time prior to 252 cal. yr B.P. (A.D. 1698);

4. Modern seasonally open marine conditions and loss of remnant ice shelves within the context of recent rapid regional warming (82 cal. yr B.P. to present; A.D. 1868 to present).

The late Holocene record from Barilari Bay is the first precisely constrained LIA glacial advance and ice shelf expansion record in Graham Land, western AP, that is concurrent with the classic definition of the LIA in the Northern Hemisphere (Lamb, 1985; Grove, 1988). Prior efforts in the western AP were inferential in terms of the actual advanced position of ice shelves and/or terrestrial termini, but no grounding limits had been defined (Domack et al., 1995, 2003; Shevenell, et al., 1996, Hall, 2007; Hall et al., 2010). The Barilari Bay sedimentary record will be greatly bolstered by results from the Site Beta ice core on the Bruce Plateau collected only 12 nautical miles east of Barilari Bay. This combined data set will provide the most direct correlation of marine sedimentary and cryospheric climatic records in Antarctica to date.

The Barilari Bay record further supports a regional LIA climate signature in the AP but highlights intra-hemispheric and global disparities in the timing and magnitude of the latest Holocene glacial advance. The overall asyn-

chronous late Holocene glacial record across the Southern Hemisphere demonstrates the issues involved in globally extrapolating the original definition of the LIA in the European Alps. In comparing glacial records across the Southern Hemisphere, there is evidence for broad late Holocene advance, but the exact timing varies according to region. The synchronicity of glacial advance in the AP, and to some degree in southern South America, during periods of abrupt and intensified cooling and sea ice growth in Arctic Canada and Iceland (A.D. 1275–1300 and A.D. 1430–1455) strengthens the case for the onset of global LIA cooling due to volcanic forcing (Miller et al., 2012), but intra-hemispheric disparities remain. The late Holocene glacial record of southern South America, however, diverges from the AP, as additional advances occurred during the classic LIA period and were progressively younger northwards. This broad asynchronous trend in the southeast Pacific sector may reflect changes in the migration of the Southern Westerlies. Late Holocene glacial behavior in New Zealand is asynchronous with the southeast Pacific, suggesting that the colder, wetter conditions of the classic LIA were not globally distributed to the southwest Pacific. While the timing of late Holocene glacial advance is asynchronous, ongoing rapid retreat over the past 150 years in the Southern Hemisphere, particularly within the AP, reaffirms that anthropogenic climate forcing is manifested globally.

ACKNOWLEDGMENTS

The data for this study were collected on the 2010 LARISSA cruise. We acknowledge the NBP10-01 Shipboard Scientific Party for field support and various discussions in and out of the field. We also thank the RV/IB *Nathanial B. Palmer* crew and Raytheon Polar Services technical personnel for the support during the cruise. We thank the National Ocean Sciences Accelerator Mass Spectrometry Facility (NOSAMS) at Woods Hole Oceanographic Institution for analysis of the radiocarbon samples used in this study. This project was funded by the National Science Foundation Office of Polar Programs awards NSF OPP ANT-0732467 to Hamilton College, NSF OPP ANT-0732625 to Colgate University, NSF OPP ANT-0732614 to University of Houston, and NSF OPP ANT-0732605 to Montclair State University, and the Korean Polar Research Institute (KOPRI) grant PP14010. We thank the students of the LARISSA short course on the Antarctic Peninsula for assisting in generating the dataset for core KC-54. Finally, we thank Joel Pederson and three anonymous reviewers for their constructive comments that greatly improved this manuscript.

REFERENCES CITED

Allen, C.S., Oakes-Fretwell, L., Anderson, J.B., and Hodgson, A., 2010, A record of Holocene glacial and oceanographic variability in Neny Fjord, Antarctic Peninsula. The Holocene, v. 20, p. 551–564, doi:10.1177/0959683609356581.

Appleby, P.G., Jones, V.J., and Ellis-Evans, J.C., 1995, Radiometric dating of lake sediments from Signy Island (maritime Antarctic): Evidence of recent climate change. Journal of Paleolimnology, v. 13, p. 179–191, doi:10.1007/BF00678106.

Balco, G., Schaefer, J.M., and LARISSA Group, 2013, Exposure-age record of Holocene ice sheet and ice shelf change in the northeast Antarctic Peninsula. Quaternary Science Reviews, v. 59, p. 101–111, doi:10.1016/j.quascirev.2012.10.022.

Bentley, M.J., Hodgson, D.A., Sugden, D.E., Roberts, S.J., Smith, J.A., Leng, M.J., and Bryant, C., 2005, Early Holocene retreat of the George VI Ice Shelf, Antarctic Peninsula. Geology, v. 33, p. 173–176, doi:10.1130/G21203.1.

Bentley, M.J., Evans, D.J.A., Fogwill, C.J., Hansom, J.D., Sugden, D.E., and Kubik, P.W., 2007, Glacial geomorphology and chronology of deglaciation, South Georgia, sub-Antarctic. Quaternary Science Reviews, v. 26, p. 644–677, doi:10.1016/j.quascirev.2006.11.019.

Bentley, M.J., Hodgson, D.A., Smith, J.A., Ó Cofaigh, C., Domack, E.W., Larter, R.D., Roberts, S.J., Brachfeld, S., Leventer, A., Hjort, C., Hillenbrand, C.D., and Evans, J., 2009, Mechanisms of Holocene palaeoenvironmental change in the Antarctic Peninsula region. The Holocene, v. 19, p. 51–69, doi:10.1177/0959683608096603.

Berkman, P.A., and Forman, S.L., 1996, Pre-bomb radiocarbon and the reservoir correction for calcareous marine species in the Southern Ocean. Geophysical Research Letters, v. 23, p. 363–366, doi:10.1029/96GL00151.

Berthier, E., Scambos, T.A., and Shuman, C.A., 2012, Mass loss of Larsen B tributary glaciers (Antarctic Peninsula) unabated since 2002. Geophysical Research Letters, v. 39, L13501, doi:10.1029/2012GL051755.

Bertrand, S., Hughen, K.A., Lamy, F., Stuut, J.B.W., Torrejon, F., and Lange, C.B., 2012, Precipitation as the main driver of Neoglacial fluctuations of Gualas glacier, Northern Patagonian Icefield. Climate of the Past, v. 8, p. 519–534.

Boldt, K.V., Nittrouer, C.A., Hallet, B., Koppes, M.N., Forrest, B.K., Wellner, J.S., and Anderson, J.B., 2013, Modern rates of glacial sediment accumulation along a 15° S-N transect in fjords from Antarctic Peninsula to southern Chile. Journal Geophysical Research, v. 118, p. 2072–2088, doi:10.1002/jgrf.20145.

Brachfeld, S.A., Banerjee, S.K., Guyodo, Y., and Acton, G.D., 2002, A 13,200 year history of century to millennial-scale paleoenvironmental change magnetically recorded in the Palmer Deep, western Antarctic Peninsula. Earth and Planetary Science Letters, v. 194, p. 311–326, doi:10.1016/S0012-821X(01)00567-2.

Brachfeld, S., Domack, E., Kissel, C., Laj, C., Leventer, A., Ishman, S., Gilbert, R., Camerlenghi, A., and Eglinton, L.B., 2003, Holocene history of the Larsen-A Ice Shelf constrained by geomagnetic paleointensity dating. Geology, v. 31, p. 749–752, doi:10.1130/G19643.1.

Brook, M.S., Neall, V.E., Stewart, R.B., Dykes, R.C., and Birks, D.L., 2011, Recognition and paleoclimatic implications of late-Holocene glaciation on Mt Taranaki, North Island, New Zealand. The Holocene, v. 21, p. 1151–1158, doi:10.1177/0959683611400468.

Charcot, J.B., 1905, The French Antarctic Expedition. The Geographical Journal, v. 26, p. 497–516, doi:10.2307/1776355.

Clapperton, C.M., Sugden, D.E., Birnie, J., and Wilson, M.J., 1989, Late-glacial and Holocene glacier fluctuations and environmental change on South Georgia, Southern Ocean. Quaternary Research, v. 31, p. 210–228, doi:10.1016/0033-5894(89)90006-9.

Cook, A.J., Fox, A.J., Vaughan, D.G., and Ferrigno, J.G., 2005, Retreating glacier fronts on the Antarctic Peninsula over the past half-century. Science, v. 308, p. 541–544, doi:10.1126/science.1104235.

Domack, E.W., 1992, Modern carbon-14 ages and reservoir corrections for the Antarctic Peninsula and Gerlache Strait area. Antarctic Journal of the United States, v. 27, p. 63–64.

Domack, E.W., and Ishman, S., 1993, Oceanographic and physiographic controls on modern sedimentation within Antarctic fjords. Geological Society of America Bulletin, v. 105, p. 1175–1189, doi:10.1130/0016-7606(1993)105<1175:OAPCOM>2.3.CO;2.

Domack, E.W., and McClennen, C.E., 1996, Accumulation of glacial marine sediments in fjords of the Antarctic Peninsula and their use as Late Holocene paleoenvironmental indicators, *in* Ross, R.M., Hofmann, E.E., and Quetin, L.B., eds., Foundations for Ecological Research West of the Antarctic Peninsula. American Geophysical Union Antarctic Research Series 70, p. 135–154, doi:10.1029/AR070p0135.

Domack, E.W., Ishman, S.E., Stein, A.B., and Jull, A.J.T., 1995, Late Holocene advance of the Müller Ice Shelf, Antarctic Peninsula: Sedimentological, geochemical and palaeontological evidence. Antarctic Science, v. 7, p. 159–170, doi:10.1017/S0954102095000228.

Domack, E.W., Leventer, A., Dunbar, R., Taylor, F., Brachfeld, S., Sjunneskog, C., Cowan, E., Daniels, J.W., Escutia, C., Evans, A., Eyles, N., Guyodo, Y., Ioio, M., Iwai, M., Kyte, F., Lauer, C., Maldonado, A., Morez, T., Osterman, L., Pudsey, C., Schuffert, J., Vigar, K., Weinheimer, A., Williams, T., Winter, D., and Wolf-Welling, T.C.W., 2001, Chronology of the Palmer Deep site, Antarctic Peninsula: A Holocene palaeoenvironmental reference for the circum-Antarctic. The Holocene, v. 11, p. 1–9, doi:10.1191/095968301673881493.

Domack, E.W., Leventer, A., Root, S., Ring, J., Williams, E., Carlson, D., Hirshorn, E., Wright, W., Gilbert, R., and Burr, G., 2003, Marine sedimentary record of natural environmental variability and recent warming in the Antarctic Peninsula, *in* Domack, E., Leventer, A., Burnett, A., Bindschadler, R., Convey, P., and Kirby, M., eds., Antarctic Peninsula Climate Variability: Historical and Paleoenvironmental Perspectives. American Geophysical Union Antarctic Research Series 79, p. 205–224.

Domack, E.W., Duran, D., Leventer, A., Ishman, S., Doane, S., McCallum, S., Amblas, D., Ring, J., Gilbert, R., and Prentice, M., 2005, Stability of the Larsen B ice shelf on the Antarctic Peninsula during the Holocene epoch. Nature, v. 436, p. 681–685, doi:10.1038/nature03908.

Ferrigno, J.G., Cook, A.J., Mathie, A.M., Williams, R.S., Jr., Swithinbank, C., Foley, K.M., Fox, A.J., Thomson, J.W., and Sievers, J., 2008, Coastal-change and glaciological map of the Larsen Ice Shelf area, Antarctica: 1940–2005. U.S. Geological Survey Geological Investigations Map I-2600-B, 1 map sheet, 28 p. text.

Flint, R.F., Sanders, J.E., and Rodgers, J., 1960, Diamictite, a substitute term for symmictite. Geological Society of America Bulletin, v. 71, no. 12, p. 1809–1810, doi:10.1130/0016-7606(1960)71[1809:DASTFS]2.0.CO;2.

Frenot, Y., Gloaguen, J.C., Picot, G., Bougere, J., and Benjamin, D., 1993, *Azorella selago* Hook. used to estimate glacier fluctuations and climatic history in the Kerguelen Islands over the last two centuries. Oecologia, v. 95, p. 140–144.

Gilbert, R., and Domack, E.W., 2003, Sedimentary record of disintegrating ice shelves in a warming climate, Antarctic Peninsula: Geochemistry Geophysics Geosystems, v. 4, no. 4, p. 1–12, doi:10.1029/2002GC000441.

Glasser, N.F., Harrison, S., Winchester, V., and Aniya, M., 2004, Late Pleistocene and Holocene palaeoclimate and glacier fluctuations in Patagonia. Global and Planetary Change, v. 43, p. 79–101, doi:10.1016/j.gloplacha.2004.03.002.

Gordon, J.E., and Harkness, D.D., 1992, Magnitude and geographic variation of the radiocarbon content in Antarctic marine life: Implications for reservoir corrections in radiocarbon dating. Quaternary Science Reviews, v. 11, p. 697–708, doi:10.1016/0277-3791(92)90078-M.

Griffith, T.W., and Anderson, J.B., 1989, Climatic control of sedimentation in bays and fjords of the northern Antarctic Peninsula. Marine Geology, v. 85, p. 181–204, doi:10.1016/0025-3227(89)90153-9.

Grove, J.M., 1988, The Little Ice Age. London and New York, Methuen, 520 p.

Grove, J.M., 2004, Little Ice Ages: Ancient and Modern. London and New York, Routledge, 718 p.

Hall, B.L., 2007, Late-Holocene advance of the Collins Ice Cap, King George Island, South Shetland Islands. The Holocene, v. 17, p. 1253–1258, doi:10.1177/0959683607085132.

Hall, B.L., 2009, Holocene glacial history of Antarctica and the sub-Antarctic islands. Quaternary Science Re-

views, v. 28, p. 2213–2230, doi:10.1016/j.quascirev.2009.06.011.

Hall, B.L., Koffman, T., and Denton, G.H., 2010, Reduced ice extent on the western Antarctic Peninsula at 700–970 cal. yr B.P. Geology, v. 38, p. 635–638, doi:10.1130/G30932.1.

Hansom, J.D., and Flint, C.P., 1989, Holocene ice fluctuations on Brabant Island, Antarctic Peninsula. Antarctic Science, v. 1, p. 165–166, doi:10.1017/S0954102089000246.

Harris, P.T., Domack, E., Manley, P.L., Gilbert, R., and Leventer, A., 1999, Andvord drift: A new type of inner shelf, glacial marine deposystem from the Antarctic Peninsula. Geology, v. 27, p. 683–686, doi:10.1130/0091-7613(1999)027<0683:ADANTO>2.3.CO;2.

Harrison, S., Winchester, V., and Glasser, N.F., 2007, The timing and nature of recession of outlet glaciers of Hielo Patagonico Norte, Chile, from their Neoglacial IV (Little Ice Age) maximum positions. Global and Planetary Change, v. 59, p. 67–78, doi:10.1016/j.gloplacha.2006.11.020.

Hodgson, D.A., Bentley, M.J., Roberts, S.J., Smith, J.A., Sugden, D.E., and Domack, E.W., 2006, Examining Holocene stability of Antarctic Peninsula ice shelves. Eos (Transactions, American Geophysical Union), v. 87, p. 305–308, doi:10.1029/2006EO310001.

Hodgson, D.A., Roberts, S.J., Smith, J.A., Verleyen, E., Sterken, M., Labarque, M., Sabbe, K., Vyverman, W., Allen, C.S., Leng, M.J., and Bryant, C., 2013, Late Quaternary environmental changes in Marguerite Bay, Antarctic Peninsula, inferred from lake sediments and raised beaches. Quaternary Science Reviews, v. 68, p. 216–236, doi:10.1016/j.quascirev.2013.02.002.

Holmlund, P., and Fuenzalida, H., 1995, Anomalous glacier response to 20th century climate changes in Darwin Cordillera, southern Chile. Journal of Glaciology, v. 41, p. 465–473.

Ingólfsson, Ó., Hjort, C., Berkman, P.A., Björck, S.E.C., Goodwin, I.D., Hall, B., Hirakawa, K., Melles, M., Möller, P., and Prentice, M.L., 1998, Antarctic glacial history since the Last Glacial Maximum: An overview of the record on land. Antarctic Science, v. 61, p. 326–344.

Jenkins, A., Dutrieux, P., Jacobs, S.S., McPhail, S.D., Perrett, J.R., Webb, A.T., and White, D., 2010, Observations beneath Pine Island Glacier in West Antarctica and implications for its retreat. Nature Geoscience, v. 3, p. 468–472, doi:10.1038/ngeo890.

Kaharoeddin, F.A., Russell, M.D., Weiterman, S.D., Cooper, C.R., Lang, T.H., Clark, D.R., Covington, J.M., Firth, J.V., Applegate, J.L., Knuttel, S., and Breza, J.R., 1988, The United States Antarctic Research Program in the western Ross Sea, 1979–1980: The sediment descriptions. Sedimentology Research Laboratory Contribution No. 53, Department of Geology, Florida State University, Tallahassee, 230 p.

Koch, J., and Kilian, R., 2005, 'Little Ice Age' glacier fluctuations, Gran Campo Nevado, southernmost Chile. The Holocene, v. 15, p. 20–28, doi:10.1191/0959683605hl780rp.

Lamb, H.H., 1985, Climatic History and the Future. Princeton, New Jersey, Princeton University Press, 835 p.

Leventer, A., Domack, E.W., Ishman, S.E., Brachfeld, S., McClennen, C.E., and Manley, P., 1996, Productivity cycles of 200–300 years in the Antarctic Peninsula region: Understanding linkages among the sun, atmosphere, oceans, sea ice, and biota. Geological Society of America Bulletin, v. 108, p. 1626–1644, doi:10.1130/0016-7606(1996)108<1626:PCOYIT>2.3.CO;2.

Leventer, A., Domack, E., Barkoukis, A., McAndrews, B., and Murray, J., 2002, Laminations from the Palmer Deep: A diatom-based interpretation. Paleoceanography, v. 17, no. 3, p. PAL 3-1–PAL 3-15.

Mann, D.H., 1986, Reliability of a fjord glacier's fluctuations for paleoclimatic reconstructions. Quaternary Research, v. 25, p. 10–24, doi:10.1016/0033-5894(86)90040-2.

Masiokas, M.H., Luckman, B.H., Villalba, R., Delgado, S., Skvarca, P., and Ripalta, A., 2009, Little Ice Age fluctuations of small glaciers in the Monte Fitz Roy and Lago del Desierto areas, south Patagonian Andes, Argentina. Palaeogeography, Palaeoclimatology, Palaeoecology, v. 281, p. 351–362, doi:10.1016/j.palaeo.2007.10.031.

McKinzey, K.M., Lawson, W., Kelly, D., and Hubbard, A., 2004, A revised Little Ice Age chronology of the Franz Josef Glacier, Westland, New Zealand. Journal of the Royal Society of New Zealand, v. 34, p. 381–394, doi:10.1080/03014223.2004.9517774.

Mercer, J.H., 1978, West Antarctic ice sheet and CO_2 greenhouse effect: A threat of disaster. Nature, v. 271, p. 321–325, doi:10.1038/271321a0.

Miller, G.H., Geirsdottir, A., Zhong, Y.F., Larsen, D.J., Otto-Bliesner, B.L., Holland, M.M., Bailey, D.A., Refsnider, K.A., Lehman, S.J., Southon, J.R., Anderson, C., Bjornsson, H., and Thordarson, T., 2012, Abrupt onset of the Little Ice Age triggered by volcanism and sustained by sea-ice/ ocean feedbacks: Geophysical Research Letters, v. 39, L02708, doi:10.1029/2011GL050168.

Milliken, K.T., Anderson, J.B., Wellner, J.S., Bohaty, S.M., and Manley, P.L., 2009, High-resolution Holocene climate record from Maxwell Bay, South Shetland Islands, Antarctica. Geological Society of America Bulletin, v. 121, p. 1711–1725, doi:10.1130/B26478.1.

Moline, M., Claustre, H., Frazer, T.K., Schofield, O., and Vernet, M., 2004, Alteration of the food web along the Antarctic Peninsula in response to a regional warming trend. Global Change Biology, v. 10, p. 1973–1980, doi:10.1111/j.1365-2486.2004.00825.x.

Morris, E.M., and Vaughn, D.G., 2003, Spatial and temporal variation of surface temperature on the Antarctic Peninsula and the limit of viability of ice shelves, *in* Domack, E., Leventer, A., Burnett, A., Bindschadler, R., Convey, P., and Kirby, M., eds., Antarctic Peninsula Climate Variability: Historical and Paleoenvironmental Perspectives. American Geophysical Union Antarctic Research Series 79, p. 61–68.

Mosley-Thompson, E., Thompson, L.G., Grootes, P.M., and Gundestrup, N., 1990, Little Ice Age (Neoglacial) paleoenvironmental conditions at Siple Station, Antarctica. Annals of Glaciology, v. 14, p. 199–204.

Mulvaney, R., Abram, N.J., Hindmarsh, R.C.A., Arrowsmith, C., Fleet, L., Triest, J., Sime, L.C., Alemany, O., and Foord, S., 2012, Recent Antarctic Peninsula warming relative to Holocene climate and ice-shelf history. Nature, v. 489, p. 141–144, doi:10.1038/nature11391.

Pudsey, C.J., and Evans, J., 2001, First survey of Antarctic sub-ice shelf sediments reveals mid-Holocene ice shelf retreat. Geology, v. 29, p. 787–790, doi:10.1130/0091-7613(2001)029<0787:FSOASI>2.0.CO;2.

Putnam, A.E., Schaefer, J.M., Denton, G.H., Barrell, D.J.A., Finkel, R.C., Andersen, B.G., Schwartz, R., Chinn, T.J.H., and Doughty, A.M., 2012, Regional climate control of glaciers in New Zealand and Europe during the pre-industrial Holocene. Nature Geoscience, v. 5, p. 627–630, doi:10.1038/ngeo1548.

Reimer, P.J., Baillie, M.G.L., Bard, E., Bayliss, A., Beck, J.W., Blackwell, P.G., Ramsey, C.B., Buck, C.E., Burr, G.S., Edwards, R.L., Friedrich, M., Grootes, P.M., Guilderson, T.P., Hajdas, I., Heaton, T.J., Hogg, A.G., Hughen, K.A., Kaiser, K.F., Kromer, B., McCormac, F.G., Manning, S.W., Reimer, R.W., Richards, D.A., Southon, J.R., Talamo, S., Turney, C.S.M., van der Plicht, J., and Weyhenmeyer, C.E., 2009, INTCAL09 and MARINE09 radiocarbon age calibration curves, 0–50,000 years cal BP. Radiocarbon, v. 51, p. 1111–1150.

Rott, H., Rack, W., Nagler, T., and Skvarca, P., 1998, Climatically induced retreat and collapse of northern Larsen Ice Shelf, Antarctic Peninsula. Annals of Glaciology, v. 27, p. 86–92.

Rymill, J.R., 1938, British Graham Land Expedition, 1934–37. The Geographical Journal, v. 91, p. 297–312, doi:10.2307/1788186.

Scambos, T.A., Hulbe, C.L., and Fahnestock, M., 2003, Climate-induced ice shelf disintegration in the Antarctic Peninsula, *in* Domack, E.W., Leventer, A., Burnett, A., Bindschadler, R., Convey, P., and Kirby, M., eds., Antarctic Peninsula Climate Variability: Historical and Paleoenvironmental Perspectives. American Geophysical Union Antarctic Research Series 79, p. 79–92.

Scambos, T.A., Bohlander, J.A., Shuman, C.A., and Skvarca, P., 2004, Glacier acceleration and thinning after ice shelf collapse in the Larsen B embayment, Antarctica. Geophysical Research Letters, v. 31, L18402, doi:10.1029/2004GL020670.

Schaefer, J.M., Denton, G.H., Kaplan, M., Putnam, A., Finkel, R.C., Barrell, D.J.A., Andersen, B.G., Schwartz, R., Mackintosh, A., Chinn, T., and Schlüchter, C., 2009, High-frequency Holocene glacier fluctuations in New Zealand differ from the northern signature. Science, v. 324,. 622–625, doi:10.1126/science.1169312.

Scherer, R.P., 1994, A new method for the determination of absolute abundance of diatoms and other silt-sized sedimentary particles. Journal of Paleolimnology, v. 12, p. 171–179, doi:10.1007/BF00678093.

Shevenell, A.E., and Kennett, J.P., 2002, Antarctic Holocene climate change: A benthic foraminiferal stable isotope record from Palmer Deep. Paleocenaography, v. 17, no. 2, p. PAL 9-1–PAL 9-10.

Shevenell, A.E., Domack, E.W., and Kernan, G.M., 1996, Record of Holocene palaeoclimate change along the Antarctic Peninsula: Evidence from glacial marine sediments, Lallemand Fjord: Papers and Proceedings of the Royal Society of Tasmania, v. 130, p. 55–64.

Skvarca, P., Rack, W., Rott, H., and Ibarzábal y Donángelo, T., 1999, Climatic trend and the retreat and disintegration of ice shelves on the Antarctic Peninsula: An overview. Polar Research, v. 18, p. 151–157, doi:10.1111/j.1751-8369.1999.tb00287.x.

Strelin, J., Casassa, G., Rosqvist, G., and Holmund, P., 2008, Holocene glaciations in the Ema Glacier Valley, Monte Sarmiento Massif, Tierra del Fuego. Palaeogeography, Palaeoclimatology, Palaeoecology, v. 260, p. 299–314, doi:10.1016/j.palaeo.2007.12.002.

Stuiver, M., and Reimer, P.J., 1993, Extended ^{14}C database and revised CALIB radiocarbon calibration program. Radiocarbon, v. 35, p. 215–230.

Stuiver, M., Denton, G.H., Hughes, T.J., and Fastook, J.L., 1981, History of the marine ice sheet in West Antarctica during the last glaciation: A working hypothesis, *in* Denton, G.H., and Hughes, T.J., eds., The Last Great Ice Sheets: New York, John Wiley and Sons, p. 319–436.

Taylor, F., Whitehead, J., and Domack, E., 2001, Holocene paleoclimate change in the Antarctic Peninsula: Evidence from the diatom, sedimentary and geochemical record: Marine Micropaleontology, v. 41, p. 25–43.

Vaughan, D.G., Marshall, G.J., Connolley, W.M., Parkinson, C., Mulvaney, R., Hodgson, D.A., King, J.C., Pudsey, C.J., and Turner, J., 2003, Recent rapid regional climate warming on the Antarctic Peninsula. Climatic Change, v. 60, p. 243–274.

Warner, N. R., and Domack, E. W., 2002, Millennial- to decadal-scale paleoenvironmental change during the Holocene in the Palmer Deep, Antarctica, as recorded by particle size analysis. Paleoceanography, v. 17, no. 3, p. PAL 5-1–PAL 5-10.

Wentworth, C.K., 1922, A scale of grade and class terms for clastic sediments. The Journal of Geology, v. 30, p. 377–392, doi:10.1086/622910.

Winkler, S., 2009, First attempt to combine terrestrial cosmogenic nuclide (^{10}Be) and Schmidt hammer relative-age dating: Strauchon Glacier, Southern Alps, New Zealand. Central European Journal of Geosciences, v. 1, p. 274–290.

Science Editor: A. Hope Jahren
Associate Editor: Joel Pederson

Manuscript Received 13 November 2013
Revised Manuscript Received 7 July 2014
Manuscript Accepted 8 August 2014

Printed in the USA